ALMA MATER STUDIORUM
UNIVERSITÀ DI BOLOGNA

DEPARTMENT OF CIVIL, CHEMICAL, ENVIRONMENTAL AND MATERIALS ENGINEERING – DICAM

MASTER'S DEGREE IN CIVIL ENGINEERING

TORSIONAL EFFECTS INDUCED BY AN ECCENTRIC WALL IN ONE-STOREY STRUCTURES

Supervisor:

Prof. Stefano Silvestri

Defended by:

Muhammad Humza Vohra

Graduation Session I / July/ 2026

Academic Year 2023–2024

Abstract

This thesis investigates the torsional effects caused by a single eccentrically positioned reinforced concrete wall in one-storey structural systems. The study is motivated by observations from the 2012 Emilia-Romagna earthquakes, during which many industrial buildings suffered severe torsional damage or collapsed because their reinforced concrete walls were located away from the building's center. When the center of stiffness is offset from the center of mass, lateral loading generates a torsional moment that increases displacement on the flexible side of the structure.

The analytical torsional amplification factor proposed by Silvestri et al. (WCEE 2024), expressed as Eq. (4), is evaluated by comparing its predictions with SAP2000 finite element results for six parametric structural models with plan aspect ratios ranging from 0.50 to 2.25. Initial validation shows that the original equation underestimates the numerical amplification factor by an average of 27.3%. Incorporating shear deformation into the wall stiffness calculation reduces the average error to 20.8%. Replacing the continuous polar stiffness term with the discrete expression, $(1/n)\ \Sigma(k_c \cdot x_i^2 + k_c \cdot y_i^2)$, produces mixed results: it significantly improves the prediction for square layouts—reducing the error to just 5.1% for Model M1 but yields less consistent improvements for rectangular configurations.

Chapter 6 investigates the reasons behind these mixed results. The analysis shows that Eq. (4) represents the torsional resistance of the column system using a single scalar polar stiffness term, without accounting for the separate contributions of the x- and y-directions. In square column grids, symmetry makes these directional contributions identical, so the simplified representation remains valid and the discrete formulation improves the prediction. In rectangular grids, however, the two directions contribute differently, meaning that a single scalar term whether continuous or discrete cannot fully capture the structural behaviour. These findings suggest that future improvements to Eq. (4) should focus on developing a direction-dependent polar stiffness formulation rather than simply replacing the continuous geometric term with a discrete one.

Keywords: torsional amplification factor, eccentric wall, one-storey structure, SAP2000, polar stiffness, continuous and discrete formulations, seismic torsion, Emilia earthquake.

Table of Contents

Chapter 1 – Introduction

1.1 Background and Motivation

On 20 and 29 May 2012, two earthquakes with magnitudes of 6.1 and 5.8 struck the Emilia-Romagna region in northern Italy. Many single-storey industrial buildings, primarily constructed using precast and cast-in-place reinforced concrete, either collapsed or suffered severe structural damage despite being designed in accordance with the seismic regulations in force at the time. Post-earthquake investigations revealed a recurring pattern: many of the damaged buildings relied on column grids combined with one or more reinforced concrete walls positioned eccentrically within the floor plan. This offset shifted the centre of stiffness away from the centre of mass, generating torsional effects during seismic loading and significantly increasing displacement demands on the flexible side of the structure.

These observations have two important engineering implications. First, an eccentrically positioned wall can generate torsional moments large enough to outweigh the benefits of its added stiffness, demonstrating that introducing a stiff wall does not always improve seismic performance. Second, they expose a limitation in the analytical tools available for preliminary structural assessment. Before the work of Silvestri et al. (2024), no closed-form solution existed for estimating torsional displacement amplification in single-storey wall–frame systems. This thesis addresses that gap by validating the proposed analytical formulation against numerical models and investigating modifications that may improve its accuracy.

Beyond their magnitude, the 2012 Emilia-Romagna earthquakes exposed critical weaknesses in a common type of industrial building. Many single-storey industrial facilities constructed between the 1970s and the early 2000s formed the backbone of manufacturing across the Po Valley. These buildings typically relied on slender precast concrete columns to support gravity loads, while lateral seismic forces were resisted by perimeter frames and reinforced concrete bracing walls. The design philosophy was simple: introducing a stiff wall into an otherwise flexible column system was expected to reduce overall lateral displacement during an earthquake.

The 2012 earthquake showed that this assumption does not always hold when the wall is positioned away from the geometric centre of the building. In many industrial structures, architectural constraints, large openings, or crane runway systems require a stiff wall to be placed along one edge of the plan. Although practical, this arrangement creates an asymmetric structural system. The centre of stiffness shifts toward the wall, while the centre of mass remains close to the geometric centre, creating structural eccentricity. During an earthquake, this eccentricity generates a torsional moment that causes the flexible side of the building to experience larger lateral displacements than would occur in a symmetric layout. A flaw in the analytical framework that practicing engineers may use to rapidly assess the amplification of torsional displacement in single-story wall-frame systems was revealed by these failures. In order to address torsional irregularity, standard seismic codes include provisions for accidental eccentricity and mandate three-dimensional analysis. They do not, however, provide closed-form tools for calculating the amount that a certain wall position increases the displacement on the flexible side relative to a symmetric reference system. The development and validation of such a tool is the primary motivation for the current thesis. The earthquake sequence also highlighted the importance of accurately modelling reinforced concrete wall stiffness in single-storey industrial buildings. Unlike the slender walls commonly used in multi-storey buildings, industrial structures often employ squat walls with height-to-length ratios close to one. In these cases, shear deformation contributes significantly to lateral displacement, meaning that a flexural-only stiffness model tends to overestimate the wall's stiffness. This affects the predicted location of the centre of stiffness and, consequently, the calculated torsional amplification factor. One of the main modifications investigated in this thesis addresses this limitation by incorporating both flexural and shear deformation into the wall stiffness calculation.

1.2 Problem Statement

This thesis focuses on predicting the ratio between the flexible-side lateral displacement of a one-storey structure with an eccentric wall and that of the same structure without the wall when subjected to a static lateral load applied at the centre of mass. This ratio, referred to as the torsional amplification factor (AF), depends on the number and stiffness of the columns, the location and stiffness of the wall, and the geometry of the structural plan. When AF exceeds one, the wall unexpectedly increases the flexible-side displacement instead of reducing it, highlighting a behaviour that challenges conventional design expectations. Silvestri et al. (WCEE 2024) used the auxiliary restraints approach to derive a closed-form formulation for AF. The main research issues of this thesis are the correctness of this expression when applied to structural models with different plan aspect ratios and the impact of two specific formula adjustments on that accuracy.

The torsional amplification factor captures the combined influence of structural eccentricity and torsional stiffness. It is defined as the ratio between the flexible-side lateral displacement of the wall–column system and the corresponding displacement of the reference column-only system under the same lateral load. An AF greater than one indicates that the wall increases flexible-side displacement, whereas a value below one indicates an overall reduction in displacement. Calculating AF analytically is challenging because the translational and rotational responses of a rigid diaphragm are coupled. To overcome this, Silvestri et al. developed the auxiliary restraints method, which temporarily restrains the diaphragm, determines the restraint forces, and then releases the restraints to recover the actual displacement. This approach separates the translational and rotational components of the response, allowing them to be calculated independently and then combined to obtain the final solution.

A further challenge is that the centre of stiffness is not fixed; it depends on the lateral load-resisting elements included in the structural model. When the wall is added to the column grid, the amount by which the centre of stiffness shifts toward the wall is governed by the ratio of the wall stiffness to the total stiffness of the column system. For this reason, the first modification investigated in this thesis focuses on improving the calculation of wall stiffness to obtain a more accurate prediction of this shift.

The equation for the torsional amplification factor also includes the polar stiffness of the column system, evaluated about the centre of stiffness. In the original formulation, this quantity is estimated using a continuous expression derived from the polar second moment of area of a uniformly distributed rectangular plan. While convenient, this approximation becomes less accurate as the column layout departs from a regular, symmetric arrangement. The second modification explored in this thesis replaces the continuous approximation with a discrete summation based on the actual positions of the columns, providing a more realistic representation of the structural system.

1.3 Objectives

The primary objective of this thesis is to evaluate the applicability and accuracy of the analytical displacement amplification factor proposed by Silvestri et al. (2024) for single-storey reinforced concrete buildings with an eccentrically positioned structural wall. The analytical formulation is assessed through comparison with detailed numerical models developed in

SAP2000 using a systematic parametric study covering six structural configurations with plan aspect ratios ranging from 0.50 to 2.25.

A second objective is to investigate potential improvements to the original analytical formulation while retaining its theoretical foundation. The first proposed modification focuses on the modelling of wall lateral stiffness. Rather than considering only flexural stiffness, the revised formulation incorporates both flexural and shear deformation, providing a more realistic representation of the squat reinforced concrete walls commonly found in industrial buildings.

The second modification examines how the polar stiffness of the column system is evaluated. In the original formulation, the column grid is represented using a continuous geometric approximation based solely on the plan dimensions. Here, that approximation is replaced with a discrete formulation that explicitly accounts for the actual locations of the columns. The analytical equation itself remains unchanged; only the geometric term used to evaluate the polar stiffness is revised, resulting in a representation that is more physically realistic.

To investigate the influence of this modification, general analytical expressions are developed for both square and rectangular column grids. The continuous and discrete formulations are evaluated for a wide range of structural configurations using spreadsheet calculations, and the convergence between the two approaches is examined as the number of columns increases. This comparison provides a rational basis for determining when the continuous approximation is sufficiently accurate and when the discrete formulation should be preferred.

Finally, the modified analytical expressions are validated against numerical results obtained from SAP2000. This comparison evaluates how each modification influences the predicted displacement amplification factor, including situations where a theoretically sound improvement does not necessarily lead to greater numerical accuracy. The findings are then used to propose recommendations for further refinement of the analytical formulation.

1.4 Scope and Limitations

The study exclusively involves single-story buildings that are subjected to linear static lateral loads in one direction. The floor diaphragm is assumed to be infinitely rigid in its plane. The wall is positioned parallel to the loading direction at the plan's right boundary. The columns are always rigid. This work does not address dynamic analysis, multi-story setups, nonlinear behavior, or multiple wall configurations.

A thorough explanation should be provided for the choice to limit the analysis to linear static response. Real displacement requirements rely on post-yield behavior, ductility demand, dynamic amplification, and ground motion frequency content since earthquake ground motion is inherently dynamic. In linear static analysis, all of these components are ignored. However, rather than providing a definitive seismic displacement estimate, the primary objective of this thesis is to validate an analytical formula for the static amplification factor. If a formula produced under linear static assumptions were compared with nonlinear dynamic findings, there would be other discrepancies unrelated to the formula's accuracy.

The analytical development and numerical validation are both carried out under the assumption of linear-elastic behaviour. Material nonlinearity, cracking, yielding, and damage accumulation are therefore excluded from the analysis. As a result, the proposed formulation is intended for preliminary structural assessment rather than for predicting the full nonlinear seismic response of real buildings.

The restriction to a single wall at the right edge of the plan parallel to the y-direction, which is the configuration for which Eq. (4) was created, represents the most common configuration observed in post-earthquake surveys. The assumption of a uniform column grid with identical bay widths in both directions may not adequately represent the behavior of actual industrial structures with varying bay spacing, even though it simplifies parametric study. The effects of non-uniform grids will be investigated in future studies.

1.5 Thesis Outline

This thesis is organised into eight chapters, each addressing a specific stage of the analytical and numerical investigation.

Chapter 1 introduces the research background, motivation, objectives and scope of the study. The importance of torsional effects in single-storey industrial buildings with eccentric structural walls is discussed together with the need for simple analytical tools capable of estimating displacement amplification during preliminary design.

Chapter 2 presents the literature review. Previous research on torsional behaviour, eccentric wall systems, analytical modelling techniques and current seismic design provisions is reviewed to establish the theoretical background for the study. Particular attention is given to the analytical framework proposed by Silvestri et al. (2024), which forms the basis of the present investigation.

Chapter 3 develops the theoretical framework adopted throughout the thesis. The assumptions of the rigid diaphragm model are introduced together with the derivation of the analytical parameters required in the displacement amplification equation. Particular emphasis is placed on the definition of the column stiffness, wall stiffness and polar stiffness of the structural system. The chapter also introduces the continuous and discrete formulations of the column-system polar stiffness that form the basis of the second modification investigated in this analysis.

Chapter 4 describes the numerical methodology adopted for validation. The SAP2000 modelling procedure, material properties, loading conditions and extraction of displacement results are presented together with the calculation procedure used to evaluate the analytical amplification factor for each model.

Chapter 5 presents the comparison between the analytical predictions and the SAP2000 numerical results for all six investigated structural models.

Chapter 6 discusses the proposed improvements to the original analytical formulation. The combined flexural-shear wall stiffness model is first evaluated, followed by the introduction of the discrete polar stiffness formulation. A general analytical comparison between the continuous and discrete formulations is then presented using square and rectangular column grids, together with a re-examination of the six SAP2000 models. Finally, recommendations are made regarding the geometric term used in the original analytical equation.

Chapter 7 discusses the engineering significance of the obtained results, the limitations of the adopted assumptions and the practical implications of the proposed modifications for structural design.

Chapter 8 summarises the principal conclusions of the research, highlights the main contributions of the study and identifies potential directions for future work.

Chapter 2 – Literature Review

2.1 Torsional Behavior in Single-Storey Structures

The torsional response of building structures under lateral loading is determined by the eccentricity between the center of mass (CM) and the center of stiffness (CS). When these two points do not coincide, a lateral force applied at the CM results in both a translational response and a rotational response about the vertical axis through the CS. The rotating component increases displacements on the flexible side of the design while decreasing those on the stiff side. The degree of this amplification is determined by the ratio of the torsional to translational natural frequencies and the structural eccentricity to the torsional radius of gyration of the system.

Chopra and Goel (1991) identified the conditions under which flexible-side displacements are most greatly amplified in their extensive examination of torsional provisions in seismic codes. Their results show that the torsional frequency of the most vulnerable systems is lower than the translational frequency. Paulay and Priestley (1992) looked at the location of the center of stiffness and the related eccentricity and found that the positioning of stiff wall sections greatly affects the system's torsional characteristics.

The torsional problem is most common in single-story industrial buildings with a single eccentric wall. This is due to the fact that techniques designed for systems with multiple scattered lateral resistive components cannot effectively manage the significant eccentricity caused by the wall's single large stiffness contribution at one plan edge. This setting is specifically addressed in Silvestri et al. (2024)'s analytical framework.

Early analytical investigations of torsional response in single-story systems characterized the floor as a rigid plate, the lateral resisting components as linear springs, and the seismic excitation as a static equivalent lateral force applied at the center of mass. The governing equations in this framework have three degrees of freedom: two horizontal translations and one rotation along the vertical axis. The main dimensionless parameters that influence the degree of flexible-side displacement amplification are the ratio of uncoupled torsional to translational natural frequency ($\Omega\theta/\Omega t$) and the ratio of structural eccentricity to torsional radius (e/r). When $\Omega\theta/\Omega t$ is less than one, torsionally flexible systems exhibit greater flexible-side amplification for a given eccentricity ratio.

De la Llera and Chopra (1994) discovered situations where static eccentricity is a reliable predictor of the dynamic torsional demand in a systematic study of the torsional response of asymmetric single-story systems under different ground motion records. They found that while static analysis usually produces a conservative estimate of flexible-side displacement for torsionally stiff systems, dynamic demand can exceed the static prediction by a factor of two or more for torsionally flexible systems. Understanding the results of the current thesis, which is entirely dependent on static analysis, depends on this distinction.

By introducing the idea of strength eccentricity, Paulay (1997) extended the mathematical foundation for torsional response beyond the elastic range. Paulay argued that designing for a low stiffness eccentricity without simultaneously controlling the strength eccentricity could result in a significant inelastic torsional demand. The nonlinear torsional response may increase if the strength eccentricity is similar in size to the stiffness eccentricity. Because the wall is typically stiffer and stronger than individual columns, this conclusion is relevant to the eccentric wall problem.

More recent experimental work on the torsional response of asymmetric reinforced concrete wall buildings by Beyer, Dazio, and Priestley (2008) shows that higher mode contributions significantly affect the dynamic torsional response of irregular systems. Although their study focused on multi-story buildings, the coupling between translational and torsional modes, the sensitivity of torsional response to the ratio of torsional to difficult mechanisms that are directly applicable to the single-story case examined in the current thesis.

The specific problem of torsion generated by a single eccentric wall in a one-story frame received relatively little analytical attention prior to the work of Silvestri et al. (2024). Since most of the analytical literature currently in publication considers systems with many lateral resisting elements, the formulas developed for systems with several lateral resisting elements distributed throughout the plan are not directly applicable to the case of a single concentrated wall element. Silvestri et al.'s auxiliary restraints method provides a closed-form solution for this configuration.

2.2 Seismic Code Treatment of Torsion

To reduce torsional impacts, Eurocode 8 (EN 1998-1, 2004) uses two strategies. To account for uncertainty in mass distribution and ground motion rotational components, the seismic force for regular structures that meet Section 4.2.3 of EC8 is subject to an accidental eccentricity equivalent to 5% of the floor dimension. A three-dimensional structural model with intrinsic torsional coupling is necessary for structures that do not meet the regularity requirements, particularly those with high structural eccentricity.

According to these criteria, one-story industrial structures with eccentric walls are often classified as torsionally irregular. However, as neither code offers explicit closed-form methods for calculating the torsional displacement amplification factor, the Silvestri et al. formula would be a useful addition to the code framework for preliminary design evaluation. Torsional impacts are addressed by contemporary seismic codes in a way that balances rigor and practicality. A fully rigorous approach would require a three-dimensional dynamic study of the actual irregular structure that considers both the spatial variation of ground motion and the interaction between translational and torsional modes. Such analysis is theoretically feasible for complex structures, but it is not feasible for the thousands of routine evaluations that are carried out annually. Simpler constraints are incorporated into seismic codes to capture the most important torsional effects while keeping tractability for ordinary engineering practice.

Eurocode 8 (EN 1998-1, 2004) specifies two conditions for torsional regularity: the radius of torsion (rt) must be greater than the radius of gyration of the floor mass (ls) in both horizontal directions, and the structural eccentricity (eo) must be greater than thirty percent of the torsional radius (rt). When both conditions are satisfied, the structure is classified as torsionally regular and can be analyzed using simplified lateral force methods with extra accidental eccentricity. A spatial model that explicitly expresses torsional coupling is required when either condition is not met.

The single-story buildings with eccentric walls studied in this thesis would normally violate the EC8 torsional regularity requirement. A system with a single dominant wall element at the plan edge typically has a torsional radius that is less than the floor mass's radius of gyration, and the wall introduces a significant stiffness asymmetry that causes the eccentricity to exceed the 30% threshold. The formula Eq. (4), which allows the engineer to quickly estimate the torsional amplification before committing to a full three-dimensional analysis, is a helpful addition to this paradigm.

The foundation of Italian seismic practice under NTC 2018 is substantially the same as that of Eurocode 8. The NTC 2018 regulations for irregular structures, which demand dynamic analysis and spatial modeling for structures that don't satisfy the regularity standards, are described in Section 7.3.3. The Circolare 7/2019 provides technical instructions for implementing NTC 2018 and explains how to evaluate torsional stiffness and calculate eccentricity for typical structural configurations. However, neither the code nor its circolare provide explicit closed-form tools for determining the flexible-side displacement amplification factor for a one-story wall-column system.

According to the widely used ASCE 7-22 standard in the United States, torsional irregularity is defined as the ratio of maximum storey drift at the plan ends to average storey drift. If this ratio is larger than 1.2, a structure is regarded torsionally irregular (Type 1a); if it is greater than 1.4, it is said to have considerable torsional irregularity (Type 1b). These thresholds pave the way for a more detailed analysis and a more exacting description of ductility. Even if the exact numerical criteria are different, the main objective of EC8 and NTC 2018 is to identify configurations where torsional effects are substantial enough to require explicit treatment during the design phase.

2.3 Prior Research on Eccentric Wall Systems

Wall-frame systems have been thoroughly examined in relation to multi-story buildings, where it is critical to distinguish between the translational stiffness of frame components and the combined flexural and shear stiffness of walls. Paulay and Priestley (1992) stress the significance of accurately accounting for all deformation mechanisms in wall sections and offer a thorough analysis of the center of stiffness in such systems. Shear deformation contributes significantly to the overall lateral deformation of squat walls common in one-story industrial structures, and the frequently used flexural-only cantilever calculation overestimates the stiffness of the wall.

In their study of the torsional behavior of symmetric and asymmetric reinforced concrete frame buildings, Brandonisio et al. (2012) showed that the degree of plan asymmetry affects the prediction error in amplification factor calculations. Their work served as the inspiration for this thesis' parametric approach, which use six models covering a range of aspect ratios to systematically assess formula accuracy rather than for a single geometric arrangement.

The lateral stiffness of structural walls has been extensively studied because of its widespread use as the primary lateral resisting mechanism in earthquake-resistant buildings. Blume, Newmark, and Corning (1961) defined the fundamental distinction between flexural and shear deformation modes in wall lateral behavior for seismic design applications based on early analytical work on reinforced concrete shear walls. For walls with height-to-length ratios significantly greater than one, flexural behavior predominates, and the cantilever formula $k_f = 3EI/H^3$ provides a precise stiffness estimate. For squat walls with ratios around or less than one, shear deformation is a major concern, requiring the combined formula that accounts for both.

The post-cracking effective stiffness of reinforced concrete walls is significantly lower than the gross-section elastic stiffness. Both ACI 318 and Eurocode 2 recommend reduced effective stiffness modifiers for cracked sections, typically in the range of 0.3 to 0.5 of gross-section values for walls with moderate axial loads. This thesis aims to validate the formula utilizing uncracked gross-section stiffness throughout, in accordance with the linear elastic analysis framework. A design application would need to include the proper stiffness reduction factors for cracking.

Magliulo, Maddaloni, and Cosenza (2012) conducted a post-seismic analysis of the torsional behavior of precast industrial buildings damaged in the Emilia earthquake to identify the structural configurations most susceptible to torsional failure. Their investigation revealed that buildings with a single wall or bracing system on one side of the design and no counterpart on the other had the largest torsional amplification of displacement. They provided qualitative recommendations for improving torsional performance but did not develop quantitative models for predicting the amplification factor. The study of Silvestri et al. (2024) explicitly addresses this highlighted need analytically.

Bosio et al. (2020) added the contribution of cladding panels to overall lateral stiffness and eccentricity to the analytical framework for single-story precast buildings. They showed how cladding, which is typically disregarded in structural studies, can greatly boost the torsional stiffness of the system, particularly when panels are arranged asymmetrically around the perimeter. The actual torsional amplification factor in a real building may differ from the formula prediction due to the stiffness contribution of the cladding, which is missing from the structural models studied here. This conclusion has implications for comprehending the current thesis's findings.

Restrepo and Rahman (2007) highlighted the importance of precisely accounting for shear deformation when assessing squat walls with aspect ratios less than two in their study of the seismic performance of cantilever reinforced concrete walls. Their experimental results showed that for walls with height-to-length ratios between 0.5 and 1.5, shear deformation accounted for 20 to 50 percent of the total lateral displacement at the elastic limit. This range, which includes the wall geometry ($H/Lw = 1.0$) used in the current thesis, provides experimental support for the inclusion of shear stiffness in the wall stiffness calculation as carried out in Modification 1. Prior studies establish the importance of stiffness eccentricity, torsional flexibility, and wall stiffness modelling, but they do not provide a simple validated closed-form predictor for the flexible-side displacement amplification of a one-storey column system with a single eccentric wall. This is the specific gap addressed by Silvestri et al. and examined in the present thesis.

2.4 The Silvestri et al. (WCEE 2024) Framework

Two comparison configurations are defined by the analytical framework that Silvestri et al. presented at the 18th World Conference on Earthquake Engineering: a reference system C that only has a regular column grid and a modified system C+W that is created by adding a single wall at the plan's right edge. The torsional amplification factor is the ratio of the flexible-side displacement of C+W to the displacement of C under the same lateral force. The derivation employs the auxiliary restraints approach, which divides the response into independent translational and rotational components by imposing additional temporary constraints on the system. AF is related to the column stiffness, wall stiffness, plan dimensions, and polar stiffness of the column distribution in the resultant closed-form expression, Eq. (4). Even though the current thesis solely concentrates on the static AF, which serves as the basis for the dynamic analysis, the article also develops a dynamic version of the amplification factor employing an energy-based Alpha method.

One of Silvestri et al.'s main conclusions is that AF might be greater than unity, especially in plan layouts where the loaded direction (y) is shorter than the perpendicular direction (x). Flexible-side displacements are larger than the translational reference due to the eccentricity-generated torsional moment. Chapter 5 of this thesis provides numerical confirmation of this outcome.

Silvestri et al.'s (WCEE 2024) analytical methodology is based on a methodical application of linear structural analysis to the specific layout of a one-story structure with one eccentric wall. The derivation begins with the definition of the reference system C (columns only) and the modified system C+W (columns plus wall). Under a unit lateral force Fy applied at the center of mass in the y-direction, the study seeks to determine the ratio of the flexible-side y-displacement in C+W to the y-displacement in C.

The supplementary constraints method works by temporarily limiting the rigid diaphragm's three degrees of freedom. Under the restrained situation, the floor-level structural elements totally oppose the applied force Fy, preventing any diaphragm motion. The restraint forces required to impose this condition are computed using the stiffness matrix of the restrained system. The real displacement is calculated by applying the negative restraint forces as a free-

body loading once the restraints are released. This decomposition allows for the separate computation and superimposition of the translational and rotational components.
The amplification factor AF (Eq. 4) is the resultant closed-form formula for the flexible-side y-displacement of the C+W system, normalized by the y-displacement of the C system. The formula has the form of a sum of two terms: a torsional contribution depending on the eccentricity, the polar stiffness of the column system, and the torsional stiffness contribution of the wall; and a direct stiffness contribution reflecting the fraction of total lateral stiffness carried by the columns alone. Whether AF is more or less than unity depends on how these parameters compete.
The study develops a dynamic amplification factor that considers the dynamic amplification of the torsional response in relation to the translational response, in addition to the static amplification factor, using an Alpha approach. The dynamic factor is represented as a change in the static factor by a frequency-dependent modification, depending on the ratio of torsional to translational natural frequency. This thesis focuses only on the static element, which forms the foundation of dynamic analysis and is realistically important for preliminary design review.
The static amplification factor formula is validated in the paper using a few numerical examples, and the results demonstrate good agreement for the configurations considered. However, neither the effect of plan aspect ratio on formula correctness nor the sensitivity to the wall stiffness model used are methodically investigated in the validation. With a parametric numerical study that systematically modifies the plan geometry across six models with aspect ratios ranging from 0.50 to 2.25, the current thesis closes these two gaps.

2.5 Damage Documentation from the 2012 Emilia-Romagna Earthquake

The post-disaster damage surveys conducted following the May 2012 Emilia-Romagna earthquake provided an unprecedented amount of factual information about the seismic sensitivity of single-story industrial facilities. In the days and weeks after the big events, a number of research teams, notably those from the University of Bologna, the University of Ferrara, and the Eucentre Foundation, undertook detailed assessments of the afflicted area. Their conclusions were published in a number of technical reports and journal articles, which contribute significantly to the body of data supporting the present view.
After inspecting over 1,200 industrial buildings in the epicentral area, Savoia et al. (2012) found that about 30% had collapsed or sustained significant damage. The most common

failure scenario was precast roof beams losing support at the column heads. Pounding between adjacent roof elements whose relative displacement during the earthquake exceeded the available support length was often the source of this. However, a significant number of the worst failures were associated with torsional irregularity, with buildings displaying asymmetric damage patterns characterized by significant damage or collapse on one side of the plan and very mild damage on the other. This pattern is consistent with the eccentric wall amplification mechanism studied in this thesis.

Magliulo et al. (2014) described several case studies of precast industrial buildings in the Emilia region that had undergone retrofitting in the years before the earthquake, often by installing reinforced concrete walls along one or two sides of the design. Some of these retrofitted structures suffered more damage than comparable unretrofitted buildings in the same area because to the torsional effects of the extra walls. This strange outcome was attributed to both the poor connection details between the new walls and the old column structure and the fact that the walls had been constructed without a corresponding analysis of the torsional repercussions.

The damage data also demonstrated the importance of the wall-to-column stiffness ratio in determining the extent of the torsional effect. Buildings where the additional wall's stiffness was either equal to or somewhat higher than the total column stiffness exhibited the greatest torsional amplification effects. Buildings with very modest wall stiffness—a flexible wall that provided no additional stiffness—or very substantial wall stiffness—a dominant wall that successfully secured one side of the building against lateral movement—showed less torsional amplification, though for different reasons. This result suggests that the sensitivity of the torsional amplification factor to the wall-to-column stiffness ratio peaks at an intermediate value, and that an analytical formula capturing this behavior could be a useful design tool for retrofit planning.

Therefore, Emilia's empirical evidence provides the justification and, in theory, the information required to validate analytical methods for torsional assessment. The earthquake demand itself is uncertain due to the unpredictable ground motion in the epicentral area, and the as-built structural characteristics of the damaged buildings are often poorly understood (cross-section dimensions, material strengths, and foundation conditions may differ from the design drawings). Since these uncertainties make direct quantitative comparison between formula predictions and observed damage difficult, the validation in this thesis is done against controlled numerical benchmarks (SAP2000) rather than empirical damage data.

2.6 Computational Methods for Torsional Analysis

Modern structural analysis programs like SAP2000, ETABS, and OpenSees provide powerful capabilities for the linear and nonlinear study of three-dimensional structural systems with torsional irregularity. These methods address the entire three-dimensional stiffness problem without the simplifications associated with closed-form analytical approaches, and they can capture features like diaphragm flexibility, higher mode contributions, and nonlinear material behavior. The current thesis uses SAP2000 as the numerical benchmark because it is widely used for this type of problem in both research and application.

The stiff diaphragm constraint feature in SAP2000, which is used in the models of this thesis, is constructed using a constraint equation that enforces the kinematic link between the master joint (at the center of mass) and all slave joints in the same diaphragm. Since this implementation is accurate in that it enforces the rigid diaphragm requirement without approximation, the numerical results serve as a true benchmark for the rigid diaphragm analytical model. The alternative approach of modeling the diaphragm as a very rigid shell element produces similar results for practical diaphragm stiffness values, but it adds a little approximation that the constraint methodology avoids.

The SAP2000 frame element formulation used for the walls and columns in this thesis is based on the Timoshenko beam theory, which considers both flexural and shear deformation. The element stiffness matrix is computed analytically for a prismatic element with uniform cross-sectional features and is accurate for the stated kinematic model (linear displacement change along the element length with constant shear strain). When the element slenderness (H/b or H/Lw) is in a range where both flexural and shear deformation are significant, this formulation can be used to the column and wall elements in the models of this thesis. Therefore, the SAP2000 element naturally captures the combined wall stiffness that is the subject of Modification 1.

For the purpose of getting displacement results, SAP2000 provides the deformed shape of the structure under the applied load, from which the y-direction displacement at every joint can be directly read. Under the stiff diaphragm constraint, the master joint displacement provides the average translational displacement of the diaphragm; however, the slave joint displacements incorporate the additional rotational contribution. The amplification factor AF_SAP is obtained by dividing the slave joint displacement at the flexible-side corner (as described in Section 4.4) by the master joint displacement of the reference system. This extraction procedure is straightforward and has negligible numerical uncertainty for linear static analysis.

Chapter 3 – Theoretical Framework

3.1 Structural Model and Assumptions

A single-story reinforced concrete building with a rigid floor diaphragm supported by a regular grid of columns makes up the structural system under investigation. A reinforced concrete wall is added at the plan's right boundary. The following presumptions are made throughout, according Silvestri et al. (2024):

• The floor diaphragm has infinite in-plane rigidity. The translational and rotational degrees of freedom are the same for every joint at floor level.

• No element has mass that resists lateral force. The center of mass, which is located at the plan's geometric centroid, is where mass is concentrated.

• At the center of mass, a static unit lateral force is applied in the y-direction.

• Every column has the same lateral stiffness (kc) in both directions; for a fixed-fixed column of height H, $kc = 12EI/H^3$.

• With very slight deformations, the structure displays linear elastic behavior.

The analytical model adopted in this study assumes a rigid floor diaphragm. In actual single-storey industrial buildings, however, the diaphragm possesses finite in-plane stiffness that depends on factors such as the roofing system, the continuity and spacing of purlins and bracing members, and the connections between the roof elements and the supporting columns. Precast industrial buildings, including those affected during the 2012 Emilia earthquake, commonly use steel or concrete beams supporting hollow-core slabs or corrugated steel sheeting. Compared with a cast-in-place reinforced concrete slab, these roof systems generally provide much lower in-plane stiffness. As a result, treating the diaphragm as perfectly rigid is a simplification that may not fully represent the behaviour of every industrial building.

However, the derivation of Eq. (4), which is based on the diaphragm's three-degree-of-freedom model, depends on the rigid diaphragm assumption. For the purposes of this thesis validating the formula and investigating modifications the assumption is adopted consistently in both the analytical model and the SAP2000 numerical model, ensuring that any discrepancy between the two is attributable to approximations within the formula itself rather than to differences in diaphragm flexibility modelling.

Assuming identical lateral stiffness in every direction is also an idealisation. In practice, precast industrial columns often have rectangular cross-sections, meaning their stiffness about the strong axis can differ substantially from that about the weak axis. In this study, only the stiffness relevant to loading in the y-direction is considered, since the wall is oriented parallel to that direction. To maintain consistency between the analytical formulation and the numerical benchmark, the SAP2000 models adopt square column sections, which provide identical lateral stiffness in both principal directions.

The decision to represent the columns as fixed-fixed members ($k_c = 12EI/H^3$) rather than fixed-pinned members ($k_c = 3EI/H^3$) reflects the assumption that each column's base and top are effectively locked against rotation. In industrial constructions, base fixity is determined by the foundation design and the quality of the connection between the precast column and the foundation cup. For well-designed cup foundations with adequate embedment depth, the base can be thought of as roughly fixed. When calculating lateral stiffness, the rigid diaphragm constraint, which restricts the rotation at the top of each column to be equal to the rotation of the diaphragm—a global degree of freedom—enforces the top fixity and produces behavior similar to a fixed-fixed column.

3.2 Reference Structural System and Definition of Stiffness Parameters

The analytical formulation developed by Silvestri et al. (2024) considers two structural configurations. The first, referred to as the reference system (C), consists of a rigid diaphragm supported exclusively by a regular grid of $(b_x+1)\times(b_y+1)$ reinforced concrete columns on a rectangular plan of dimensions $L_x \times L_y$ with uniform bay widths. The second, referred to as the modified system (C+W), is obtained by introducing a reinforced concrete wall along one edge of the building while maintaining the original column layout. The displacement amplification factor is defined as the ratio between the flexible-side displacement of the modified system and the displacement of the reference system subjected to the same lateral load.

Because the rigid diaphragm forces all structural elements to undergo identical in-plane translations and rotations, the lateral behaviour of the structure may be represented by three degrees of freedom: translation in the x-direction, translation in the y-direction, and rotation about the vertical axis through the diaphragm centre of mass.

To avoid confusion, two different stiffness quantities are distinguished throughout this thesis. The first is the lateral stiffness of an individual column, denoted $k_{c,single}$ (referred to simply as k_c throughout the remainder of this chapter). Assuming fixed–fixed end conditions and linear elastic behaviour, the lateral stiffness of a single column is $k_c = 12EI/H^3$, where E is the Young's modulus of concrete, I is the second moment of area of the column cross-section, and H is the column height. The second quantity is the total lateral stiffness of the complete column system, denoted $K_{c,tot}$. For a system consisting of n identical columns, the displacement of the reference system under a lateral force F_y applied at the centre of mass is given by:

$$u_{y,C} = F_y / (n \cdot k_c) \quad (3.1)$$

Since the geometric centroid of the column grid and the centre of stiffness coincide in the reference system, this is a pure translation with no rotation, and the total lateral stiffness is $K_{c,tot} = n \cdot k_c$. Throughout the remainder of this thesis, lower-case k always refers to the stiffness of a single structural element, whereas upper-case K represents the combined stiffness of a complete structural system; this notation is adopted consistently to avoid confusion when developing the analytical expressions.

The polar stiffness of the column system about its centroid, denoted $I_{pk,CS}$ (the subscript CS denoting Column System), is defined in discrete form as the sum of each column's stiffness contribution weighted by the square of its distance from the centroid,

$$I_{pk,CS} = \Sigma_i \, k_c \cdot (x_i^2 + y_i^2) \quad (3.2)$$

and is approximated in continuous form by treating the column stiffness as uniformly distributed over the plan area,

$$I_{pk,CS} = k_c \cdot (L_x^2 + L_y^2) / 12 \quad (3.3)$$

Equation (3.3) corresponds to the polar second moment of area of a uniformly distributed rectangular plate with plan dimensions $L_x \times L_y$. Although this continuous representation is convenient for analytical derivations, it differs from the exact discrete expression given in Eq. (3.2) when the column grid is relatively coarse. As demonstrated in Section 3.6 and verified numerically in Chapter 6, the two formulations converge as the number of columns increases and the grid becomes progressively finer.

The polar stiffness represents the resistance offered by the column layout against rotation of the rigid diaphragm: a high polar stiffness indicates that the columns collectively resist diaphragm rotation, lowering the flexible-side displacement amplification, while a low polar stiffness relative to the eccentricity produces substantial torsional amplification. For a square plan ($L_x = L_y = L$), Eq. (3.3) reduces to $I_{pk,CS} = k_c \cdot L^2/6$, showing that the continuous polar stiffness scales with the square of the plan dimension and, notably, does not depend on the number of columns — a simplification whose consequences are examined in Section 3.6.

The wall provides an additional lateral stiffness, denoted kwk. Unlike the original formulation, which considered only flexural stiffness, the present study adopts the combined flexural–shear stiffness derived in Section 3.5. Accordingly, the total lateral stiffness of the modified structural system is $K_{CW} = K_{c,tot} + k_w$, where K_{CW} represents the stiffness of the complete wall–column system. With these definitions established, all stiffness quantities used in the analytical formulation are clearly identified before introducing the centre of stiffness, structural eccentricity, and displacement amplification factor in Sections 3.3 and 3.4.

3.3 Modified System — Columns Plus Eccentric Wall (Model C+W)

Adding the wall at position $x = L_x$ with y-direction stiffness $k_{y,w}$ shifts the centre of stiffness to:

$$x_{CK} = (\Sigma\, k_c \cdot x_i + k_{y,w} \cdot L_x) / (n \cdot k_c + k_{y,w}) \qquad (3.4)$$

Establishing a structural eccentricity $e_K = |L_x/2 - x_{CK}|$ between the new CS and the CM. A torsional moment $M_\theta = F_y \bullet e_K$ about the CS is produced by the lateral force F_y applied at CM. At $x = 0$, the side across from the wall, the flexible-side y-displacement is:

$$u_{y,F} = u_{y,trans} + \theta \cdot x_{CK} \qquad (3.5)$$

Where θ is the diaphragm rotation. The amplification factor is:

$$AF = u_{y,F} / u_{y,C} \qquad (3.6)$$

The movement of the centre of stiffness can be understood by modelling the wall as an additional, highly stiff spring located at $x=L_x$. In a system of parallel springs, the centre of stiffness corresponds to the stiffness-weighted average of the spring locations. For the column-only system, all columns have identical stiffness and are arranged symmetrically, so this point coincides with the geometric centroid. Once the wall is introduced at the edge of the plan, the stiffness distribution becomes asymmetric, causing the centre of stiffness to shift towards the wall by an amount governed by the ratio to $k_{y,w}/(n \bullet k_c + k_{y,w})$.

The structural eccentricity (e_K) is defined as the distance between the centre of stiffness x_{CK} and the centre of mass, which lies at $x=L_x/2$ for a symmetric plan. When a positive lateral

force acts in the y-direction through the centre of mass, it produces a clockwise torsional moment about the centre of stiffness. Consequently, the side adjacent to the wall (x=Lx) undergoes less displacement than the average translational movement of the diaphragm, whereas the opposite side (x=0) experiences a larger displacement.
The polar stiffness of the C+W system differs from that of the reference column system in two respects. First, the wall contributes an additional torsional stiffness term, kθ,w, which depends on both its lateral stiffness and its distance from the new centre of stiffness, xCK. Second, the reference point shifts from the centroid of the original column grid to the updated centre of stiffness. For the structural configuration considered in this thesis, where the wall is located along the edge of the plan, the polar stiffness of the column system, Ipk,C, remains the dominant contribution, while the wall adds only a relatively small increase to the overall torsional resistance.

3.4 Analytical Formula — Eq. (4)

The analytical displacement amplification factor proposed by Silvestri et al. is expressed as a function of the stiffness distribution within the structural system. The equation combines the contribution of the column system, the additional stiffness introduced by the eccentric wall, and the torsional resistance associated with the distribution of the columns about the centre of stiffness.

To avoid ambiguity, the notation introduced in Section 3.2 is adopted throughout the derivation. The stiffness of a single column is denoted by kc, while the total lateral stiffness of the column system is Kc,tot=nkc. The polar stiffness of the column system, Ipk,CS, may be evaluated either using the continuous approximation of Eq. (3.3), as proposed by Silvestri et al., or using the exact discrete formulation of Eq. (3.2), which is based on the actual column coordinates. As discussed in Section 3.6, the present study does not alter the analytical form of the amplification equation. Instead, only the geometric term used to evaluate the column-system polar stiffness is replaced, preserving the original derivation while providing a more representative description of the actual column layout.

The original analytical equation is therefore first presented exactly as proposed by Silvestri et al., using the continuous polar stiffness of Eq. (3.3), before the two modifications investigated in this research are introduced in Chapter 6:

$$AF = [Ex,c / ((1/n) \cdot \Sigma(xi^2 + yi^2) + Ex,c^2 + k\theta,w/ky,c)] \cdot (Lx/2 + Ex,c) + ky,c/(ky,c + ky,w) \quad (3.7)$$

where ky,c = n•kc is the total column stiffness in y, ky,w is the wall y-stiffness, kθ,w is the torsional stiffness contribution of the wall, and Ex,c is the x-distance from the column grid centroid to the rightmost column (equal to Lx/2 for a symmetric grid). In keeping with the original paper notation, this expression is referred to as Eq. (4) throughout.

The two terms on the right side of Equation (4) have distinct physical meanings. The second formula, ky,c/(ky,c + ky,w), is the portion of the total system y-stiffness generated by the columns alone. The displacement of the C+W system is equal to that of the C system (AF = 1) in the absence of the wall, as this factor approaches unity as the wall stiffness ky,w approaches zero. This amount decreases as ky,w increases relative to ky,c, suggesting that the wall is carrying a larger percentage of the applied force. The idea that increasing stiffness reduces displacement is consistent with the fact that this term alone constantly yields AF < 1. The first component of the equation represents the torsional correction and depends on the eccentricity Ex,c, the polar stiffness, and the wall's torsional stiffness contribution. For a perfectly symmetric system (Ex,c=0), this term becomes zero, reducing the amplification factor to the direct stiffness ratio alone. As the eccentricity increases—for example, as the wall stiffness increases while its position remains unchanged—the torsional contribution also grows. Whether the overall displacement amplification increases or decreases depends on the balance between this positive torsional effect and the reduction produced by the direct stiffness term. When the torsional contribution becomes dominant, the amplification factor exceeds unity (AF>1).

A larger polar stiffness corresponds to greater torsional resistance of the column system. Consequently, the diaphragm undergoes less rotation under a given torsional moment, reducing the torsional contribution to the flexible-side displacement. This moderating effect is reflected by the polar stiffness term in the denominator of the first component of Eq. (4). Accordingly, when the discrete polar stiffness is used, models with larger values of Lx do not necessarily produce smaller prediction errors. Although the discrete value of Ix increases with plan width, the equation depends on the combined quantity Ix+Iy. For elongated plans, Iy remains relatively small, so the total discrete polar stiffness does not increase as much as the continuous approximation would suggest.

3.5 Wall Stiffness — Combined Shear and Flexural

Shear and flexural deformations working in tandem give the reinforced concrete wall its y-direction rigidity. Regarding a wall with height H, length Lw, thickness tw, shear modulus G, and elastic modulus E:

$$k_f = 12EI / H^3 \qquad \text{(flexural stiffness)} \qquad (3.8)$$

$$k_s = G \cdot A_v / H \qquad \text{(shear stiffness)} \qquad (3.9)$$

$$1/k_w = 1/k_f + 1/k_s \qquad (3.10)$$

Where $I = t_w \cdot L_w^3/12$ and $A_v = 0.833 \cdot t_w \cdot L_w$ (rectangular section shear area factor 5/6). The original formula uses kf only; Modification 1 uses the combined kw from Eq. 3.10.

The combined stiffness expression follows directly from the fact that flexural and shear deformations act in series. When a lateral load is applied to the top of a wall cantilever, the total lateral displacement is the sum of the bending and shear components. Bending produces the familiar curved deflected shape of a cantilever, whereas shear results in a nearly linear displacement profile. Because these deformation modes act in series, the equivalent lateral stiffness is obtained from the harmonic combination of the individual flexural and shear stiffnesses, with each stiffness defined as the inverse of the displacement produced by a unit lateral load.

For a wall with height H = 4 m and length Lw = 4 m (H/Lw = 1.0), the ratio of shear to flexural stiffness is $k_s/k_f = (G \cdot A_v \cdot H^2)/(3E \cdot I)$. The geometric properties ($A_v = 0.833 \cdot t_w \cdot L_w = 0.667$ m² $I = 0.2 \cdot 4^3/12 = 1.067 \cdot 10^{-3}$ m²) and material properties (E = 30 GPa, G = 12.5 GPa). This extraordinarily high ratio suggests that, for this wall shape, shear stiffness is significantly greater than flexural stiffness. Consequently, the shear correction is negligible (less than 1%), and the flexural component governs almost all of the total stiffness. Nonetheless, the modification is physically correct and is made for generality and completeness.

The correction becomes more crucial for walls with smaller H/Lw ratios (squatter walls) or lower shear modulus relative to elastic modulus. For reinforced concrete with G/E = 0.42, only abnormally squat walls with H/Lw < 0.3 have a shear correction greater than 5%. Although the correction is minimal for the wall geometry used in the current models (H/Lw = 1.0), the combined formula is frequently employed since it represents the physically realistic model and ensures that the formula is applicable to a larger variety of wall geometries without alteration.

Both flexural and shear deformations are inherently included in the stiffness formulation of the SAP2000 frame element. Consequently, no additional modelling modifications are required, as the finite element model automatically accounts for the combined wall stiffness. Any difference between the SAP2000 results and the original analytical formulation, which considers only flexural stiffness, therefore includes the influence of shear deformation. By replacing kf with the combined stiffness kw, Modification 1 brings the analytical model into closer agreement with the numerical benchmark because both approaches represent the same underlying structural behaviour.

3.6 Polar Stiffness of the Column System: Continuous and Discrete Formulations

The polar stiffness of the column system represents the resistance offered by the column layout against rotation of the rigid diaphragm. Since torsional displacement depends not only on the total stiffness of the columns but also on their positions relative to the centre of stiffness, an accurate evaluation of the polar stiffness is essential for predicting the displacement amplification factor.

Although Eq. (3.3) provides a simple and practical approximation of the column-system polar stiffness, it is based on the assumption that lateral stiffness is uniformly distributed over the entire building plan. In actual structures, however, stiffness is concentrated at discrete column locations rather than distributed continuously. Therefore, the continuous approximation may not accurately represent the polar stiffness of buildings with relatively sparse column grids. To examine this limitation, this section introduces a discrete formulation based on the actual column coordinates while maintaining the original analytical framework.

For a structure containing n identical columns, each having stiffness kc, the discrete polar stiffness of Eq. (3.2) may be normalised by the number of columns to give a per-column average geometric term,

$$\mathrm{Ipk,CS,disc} = \mathrm{Kc,tot} \cdot [\,(1/n) \cdot \Sigma_i\,(xi^2 + yi^2)\,] \quad (3.11)$$

where xi and yi are the coordinates of the i-th column measured from the centroid of the column grid. This form highlights that the total stiffness term, Kc,tot, is identical to that of the continuous formulation of Eq. (3.3); the only difference lies in the geometric term, which changes from the continuous approximation $(Lx^2+Ly^2)/12$ to the discrete average

$(1/n)\cdot\Sigma(xi^2+yi^2)$. Consequently, the only modification introduced by adopting the discrete formulation is the replacement

$$(Lx^2 + Ly^2)/12 \rightarrow (1/n) \cdot \Sigma_i (xi^2 + yi^2) \quad (3.12)$$

This substitution maintains the mathematical structure of the original equation while replacing the continuous approximation with the exact average squared distance of the columns from the centroid. Unlike the continuous approach, the discrete expression directly considers the actual locations of the structural elements. This difference becomes particularly important for coarse column grids, where the stiffness is concentrated at a limited number of locations rather than distributed uniformly throughout the plan.

To evaluate the effect of this substitution, general analytical expressions were developed for both square and rectangular column grids and implemented in a Microsoft Excel spreadsheet. The spreadsheet evaluates the continuous and discrete formulations for different column arrangements while maintaining a constant bay spacing of 4 m. The results, discussed in Chapter 6 and Appendix E, show a clear convergence trend. For coarse grids with a limited number of columns, the difference between the two formulations is significant because the continuous approximation does not fully capture the actual discrete stiffness distribution. As the number of columns increases, the discrete arrangement approaches a continuous stiffness field and the difference gradually reduces.

For the square grids investigated in this formulation, the percentage difference decreases from approximately 50% for a 3×3 column layout to approximately 9.5% for a 20×20 grid, to about 2% for a 100×100 grid and approximately 0.2% for a 1000×1000 grid. A similar convergence trend is observed for rectangular grids, although the rate of convergence also depends on the plan aspect ratio. These results demonstrate that the continuous formulation represents the limiting case of the discrete formulation as column spacing tends to zero: the geometric term $(Lx^2+Ly^2)/12$ adopted by Silvestri et al. is the continuous limit of the discrete average $(1/n)\cdot\Sigma(xi^2+yi^2)$. This establishes the theoretical relationship between the two formulations, and it is examined numerically — including its effect on the predicted amplification factor — in Chapter 6.

3.7 Summary of the Theoretical Framework

This chapter has presented the theoretical framework adopted throughout the thesis for evaluating the displacement amplification factor of single-storey reinforced concrete buildings with an eccentric structural wall.

The analytical model is based on a rigid diaphragm supported by a regular column grid, with the wall providing an additional source of lateral stiffness and eccentricity. To ensure consistency throughout the derivation, a clear distinction has been established between the stiffness of an individual column, $k_{c,single}$, and the total stiffness of the complete column system, $K_{c,tot}$.

Two modifications to the original analytical formulation have been introduced. The first replaces the flexural-only wall stiffness with a combined flexural-shear stiffness (Section 3.5), providing a more representative estimate of the lateral behaviour of squat reinforced concrete walls. The second replaces the continuous approximation used to evaluate the polar stiffness of the column system with a discrete formulation based on the actual coordinates of the columns (Section 3.6).

Unlike the original study, where the polar stiffness is evaluated using an equivalent continuous stiffness distribution, the present work shows that the analytical equation itself can be maintained by modifying only the geometric term associated with the column arrangement. The overall structural stiffness remains unchanged, while the geometric contribution can be calculated directly from the actual column coordinates.

This modification is further investigated in Chapter 6, where the continuous and discrete formulations are compared through general analytical expressions, a spreadsheet-based parametric study, and a reassessment of the six SAP2000 models previously used for validation in Chapter 5. Although the convergence between the two polar stiffness formulations defines the applicability range of the continuous approximation, the effect of this convergence on the accuracy of displacement amplification predictions must be evaluated separately for the structural configurations considered in this thesis.

For ease of reference, Table 3.1 summarises the notation introduced in this chapter.

Symbol	Meaning
$k_{c,single}$ (k_c)	Lateral stiffness of a single column
$K_{c,tot}$	Total lateral stiffness of the column system (= $n \cdot k_c$)

Symbol	Meaning
kw	Combined flexural-shear lateral stiffness of the wall
KCW	Total lateral stiffness of the wall-column system (= Kc,tot + kw)
n	Total number of columns
xi, yi	Coordinates of column i, measured from the column-grid centroid
Ipk,CS	Polar stiffness of the column system about its centroid
Ipk,CS,cont	Continuous approximation of the polar stiffness, Eq. (3.3)
Ipk,CS,disc	Discrete formulation of the polar stiffness, Eq. (3.11)
xCK	x-coordinate of the centre of stiffness of the C+W system
eK	Structural eccentricity between centre of stiffness and centre of mass
AF	Displacement amplification factor, uy,F / uy,C

3.8 Derivation of the Centre of Stiffness for the C+W System

For a structural system subjected to lateral loading, the centre of rigidity is the point about which the diaphragm undergoes pure rotation under an applied torsional moment and pure translation when a lateral force is applied through that point. For the column-only reference system C, the centre of stiffness is obtained by imposing equilibrium of the stiffness moments about this point in both the x- and y-directions.

For a column-only system with n uniformly distributed columns of stiffness kc on a rectangular grid, the x-coordinate of the center of stiffness is the stiffness-weighted average of the column x-positions: $x_{CS,C} = (\Sigma_i\, kc) \cdot xi) / (n \cdot kc) = (\Sigma_i\, xi)/n$. For a rectangular grid that is regular and has columns at xi = i The sum of sites is $\Sigma_i\, xi = (0 + dx + 2dx + ... + bx \cdot dx)$ for i = 0, 1,..., bx, where dx = Lx/bx.•(by+1) = dx•bx•(bx+1)/2•(by+1). By dividing by n = (bx+1)(by+1), xCS,C = dx•bx/2 = Lx/2. This confirms that the geometric centroid of the plan is the center of stiffness of the column-only system, as stated in Section 3.2.

At position x = Lx, the wall increases the stiffness ky,w for the C+W system. The x-coordinate of the center of stiffness of the C+W system is as follows: xCS,CW = (n•kc•xCS,C + ky,w•Lx) / (n•kc + ky,w) = (n•kc•Lx/2 + ky,w•Lx) / (n•kc + ky,w) = Lx•(n•kc/2 + ky,w) / (n•kc + ky,w). This can be expressed as xCS,CW = Lx/2 + Lx•ky,w / (2•(n•kc + ky,w)), showing that the center of stiffness is always to the right of the plan centroid (x = Lx/2) for ky,w > 0 and that the shift rises monotonically with ky,w.

Structural eccentricity is defined as $eK = Lx/2 - xCS,CW$ (the distance between the center of stiffness and the center of mass at $x = Lx/2$), which is negative (i.e., the center of stiffness is to the right of the center of mass): $eK = -Lx \cdot ky,w / (2 \cdot (n \cdot kc + ky,w))$. The amplitude of the eccentricity, $|eK| = Lx \cdot ky,w / (2 \cdot (n \cdot kc + ky,w))$, increases from zero (no wall) to $Lx/2$ (infinitely stiff wall, which would push the center of stiffness all the way to $x = Lx$). Eccentricities between 0.17 and•Lx to 0.33•Lx are found for the wall-to-column stiffness ratios typical of the models in this thesis when $ky,w/(n \cdot kc)$ is of order 0.5 to 2.
The wall does not shift the center of stiffness in the y-direction since it is parallel to y and adds no x-direction stiffness. Consequently, $yCS = Ly/2$ (the centroid of the column grid in y) is the y-coordinate of the center of stiffness for both C and C+W systems. This shows that when a lateral force in the y-direction is applied at the center of mass (also at $y = Ly/2$), there is no eccentricity in the y-direction and no torsional coupling arises from y-direction eccentricity. The torsional coupling originates solely from the above-derived x-direction eccentricity eK.

3.9 Derivation of the Torsional Amplification Factor

After determining the center of stiffness, the torsional amplification factor can be computed using the rigid diaphragm model's three-degree-of-freedom stiffness equations. Using the center of stiffness as the reference point, the three equations of equilibrium for the diaphragm under a unit lateral force $Fy = 1$ applied at the center of mass (which is offset from the center of stiffness by eK in the x-direction) are as follows: $Kx \cdot ux = 0$, $Ky \cdot uy = 1$, $K\theta \cdot \theta = eK$, where Kx and Ky are the total translational stiffnesses in x and y, $K\theta$ is the torsional stiffness about the center of stiffness, and ux, uy, and θ are the diaphragm translations and rotation.
Since the translational stiffness in the y-direction is $Ky = n \cdot kc + ky,w$ (the total of all y-direction stiffnesses), the average translational displacement in y is $uy,avg = 1/Ky = 1/(n \cdot kc + ky,w)$. $K\theta = \Sigma_i kc \cdot (xi - xCS,CW)^2 + ky,w \cdot (Lx - xCS,CW)^2 + \Sigma_i kc \cdot (yi - yCS)^2 = n \cdot kc \cdot (Ipk,C + \Delta Ipk) + k\theta,w$, where Ipk,C is the column system's polar stiffness about the column centroid and ΔIpk takes into account the change of reference point from the column centroid to the center of stiffness.
The diaphragm's rotation under the unit lateral force applied at the center of mass is represented as $\theta = eK/K\theta$. The y-displacement at the flexible side ($x = 0$) with respect to the center of stiffness is equal to the average translational displacement plus the rotational displacement: $uy,F = uy,avg + \theta \cdot xCS, CW = 1/Ky + (eK/K\theta) \cdot xCS,CW$. Normalising by the

reference displacement uy,C = 1/(n•kc) gives the amplification factor AF = uy,F/uy,C = n•kc/Ky + n•kc•eK•xCS,CW/Kθ, which is Eq. (4) in the notation of Silvestri et al. (2024) after substituting the expressions for Ky, eK, xCS,CW, and Kθ in terms of the column stiffness kc, the wall stiffness ky,w, the plan dimensions Lx and Ly, and the polar stiffness Ipk,C.

Chapter 4 – Numerical Modelling in SAP2000

4.1 Parametric Study Overview

In SAP2000, six structural models M1–M6 encompassing plan aspect ratios Ly/Lx between 0.50 and 2.25 were built. Every model has a storey height of four meters and a bay width of four meters in both directions. One bay at the right border (x = Lx), parallel to y, is occupied by a single reinforced concrete wall. The geometric properties are summarized in Table 4.1.

Model	Bays X	Bays Y	Lx (m)	Ly (m)	n columns	Ly/Lx
M1	3	3	12	12	16	1.00
M2	4	5	16	20	30	1.25
M3	10	5	40	20	66	0.50
M4	4	9	16	36	50	2.25
M5	9	5	36	20	60	0.56
M6	5	9	20	36	60	1.80

Table 4.1 – Geometric properties of the six parametric models.

The six parametric models were chosen to cover a representative range of plan aspect ratios while keeping the number of models manageable for detailed individual study. Ly/Lx ranges from 2.25 (M4, a tall plan with Lx = 16 m and Ly = 36 m) down to 0.50 (M3, a wide plan with Lx = 40 m and Ly = 20 m). This spread includes wide-plan cases where AF > 1 is predicted by the analytical formula, and tall-plan cases where the wall is expected to produce a net reduction in displacement. The square-plan model M1 (Lx = Ly = 12 m) serves as the baseline, where the continuous and discrete polar stiffness formulas should agree most closely.

Using a constant 4 m bay width in both directions means the main variable distinguishing the models is the number of bays, not a mix of bay spacing and bay count — which makes it easier to isolate the effect of plan aspect ratio. Column count n ranges from 16 (M1, a 4×4 grid) to 66 (M3, an 11×6 grid). This matters for Modification 2, since the (1/n) normalization in the discrete polar stiffness depends on both grid size and column count.

Columns in single-story industrial buildings used for light manufacturing and warehousing in the Po Valley are usually four meters high. The smaller columns used in these buildings, which are principally dimensioned for seismic lateral loading, have a cross-section of 300 x 300 mm. The choice of column cross-section has no bearing on the main conclusions of the thesis, and as all data are normalized by the column stiffness kc in the computation for the amplification factor, the absolute value of kc does not alter the computed AF.
The parametric study is methodical rather than exhaustive. A more complete analysis would test additional aspect ratios (e.g., $L_y/L_x = 0.33, 0.67, 1.5, 3.0$), and would also vary the wall's position and stiffness. The six models here strike a reasonable balance between coverage and computational effort while still supporting the thesis's main conclusions: the systematic underestimation of AF, the improvement from Modification 1, and the geometry-dependent behavior of Modification 2.

4.2 Element Properties and Boundary Conditions

Every column is represented as a frame element with square cross-sections of 300 × 300 mm, concrete elastic modulus $E = 30$ GPa, and fixed base conditions, which are characteristics common to industrial columns. The floor diaphragm is imposed at a master joint at the plan centroid (center of mass) as a strict constraint. The wall is a frame part that is fastened at the base and has a cross-section of 200 mm by 4000 mm.
A master-slave constraint enforces the rigid diaphragm at each floor level in SAP2000. For each model, the master joint sits at the center of mass — which coincides with the geometric centroid of the column grid. All floor-level joints are slaved to the master joint's translations and rotation in the horizontal plane, enforcing the rigid diaphragm assumption numerically and keeping the SAP2000 results directly comparable to the analytical model.
The reinforced concrete wall is represented as a single frame element that stretches from the base to the floor level, with a rectangular cross-section of width $t_w = 200$ mm and depth $L_w = 4000$ mm. The element is oriented so that its strong axis is parallel to the y-direction (the loading direction) and given predetermined boundary conditions at the base. The gross-section elastic characteristics ($E = 30$ GPa, $G = 12.5$ GPa, $I = 1.067\times10^{-3}$ m² $A_v = 0.667$ m²) are applied for cracking without stiffness reduction in compliance with the linear elastic analysis framework.
Columns are frame elements with 300×300 mm square cross-sections, sharing the same material properties as the wall ($E = 30$ GPa, $G = 12.5$ GPa). Bases are fixed (all six DOFs

restrained), matching the analytical model's fixed-fixed assumption. The master-slave constraint ties each column top's rotation to the master joint, reproducing the fixed-fixed condition used in $kc = 12EI/H^3$.

The wall top joint is slaved to the diaphragm along with the column tops, so the diaphragm distributes force to each element in proportion to its stiffness, with wall and columns moving as one rigid body. Since there's no moment release at this connection, the wall behaves as fixed-fixed between base and diaphragm.

4.3 Loading and Analysis

Under unit lateral force $Fy = 100$ kN applied in the y-direction at the diaphragm master joint, linear static analysis was carried out. There is no gravity load. The derivation of Eq. (4), which is predicated on unit lateral force at the center of mass, is in line with this. A 1 kN point load is applied at the master joint in the positive y-direction, with no moment, since the center of mass and the point of load application coincide. The lateral-resisting elements then pick up force in proportion to their stiffness and distance from the center of stiffness.

The SAP2000 linear static analysis solves the system of simultaneous equations $Ku = F$, where K is the built stiffness matrix, u is the vector of nodal displacements, and F is the vector of applied nodal forces. Because the rigid diaphragm constraint restricts the effective number of degrees of freedom from the entire nodal count to three (two translations and one rotation of the master joint), the effective stiffness matrix is a 3x3 matrix for each storey. The quantities of interest are derived from the displacements at each node obtained from the solution for u.

The linear static analysis is carried out twice for each of the six structural models: once for the reference system C (columns only, no wall) and once for the modified system C+W (columns plus eccentric wall). The wall element's presence or absence is the only variation between the two analyses, which apply the same mesh, boundary conditions, and loading. This paired-analysis approach ensures that any systematic numerical errors are removed when computing the ratio $u_{y,F}/u_{y,C}$. Therefore, the amplification factor AF_SAP simply represents the structural behavior of the system.

4.4 Displacement Extraction

For each model, two displacements are extracted: uy,F from the irregular model (with wall) at the flexible-side corner joint at (x=0, y=0) and uy,C from the reference model (no wall) at the master joint. The amplification factor in numbers is:

$$AF\_SAP = u_{y,F} / u_{y,C} \tag{4.1}$$

MODEL M1 — 3×3 bays | Lx=12m, Ly=12m | Ly/Lx=1.00

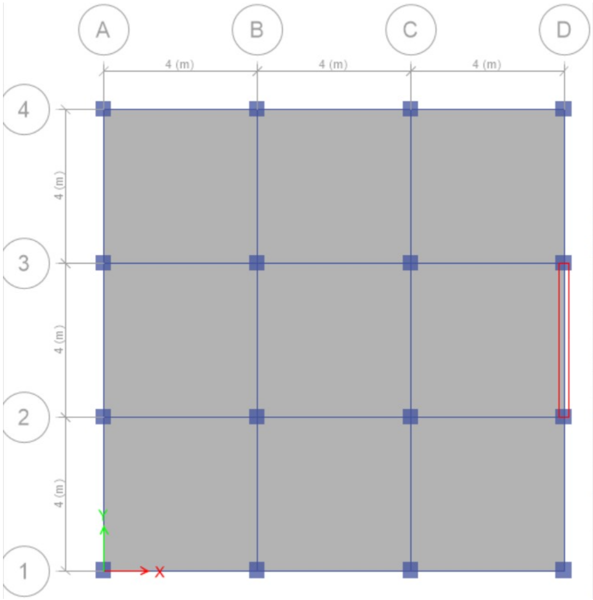

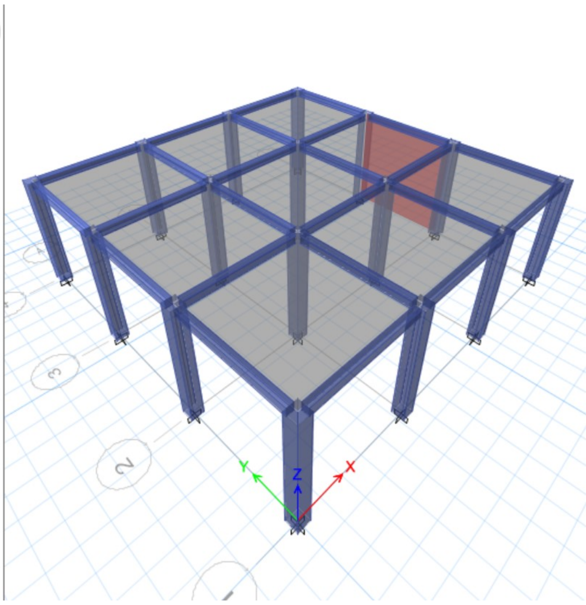

MODEL M2 — 4×5 bays | Lx=16m, Ly=20m | Ly/Lx=1.25

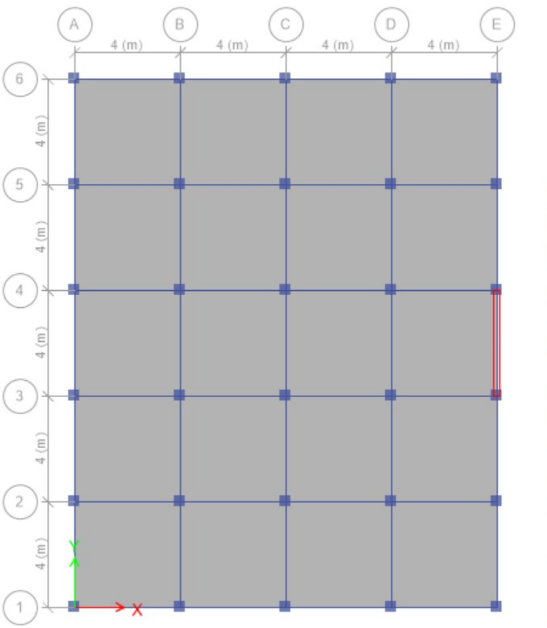

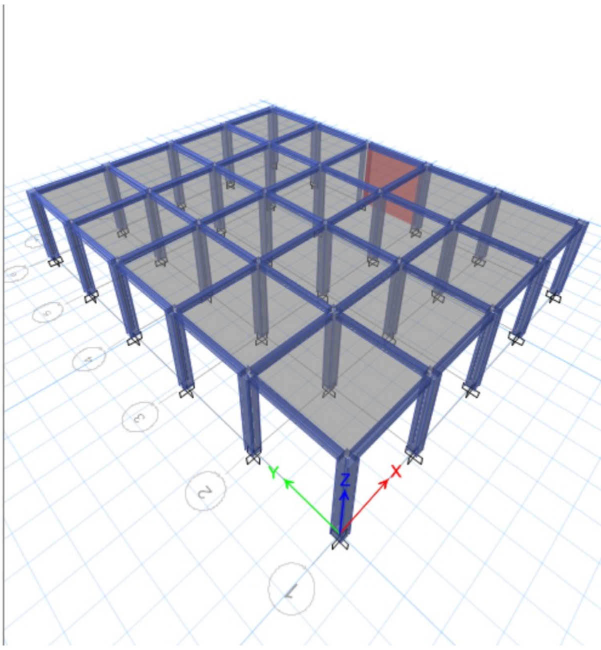

MODEL M3 — 10×5 bays | Lx=40m, Ly=20m | Ly/Lx=0.50

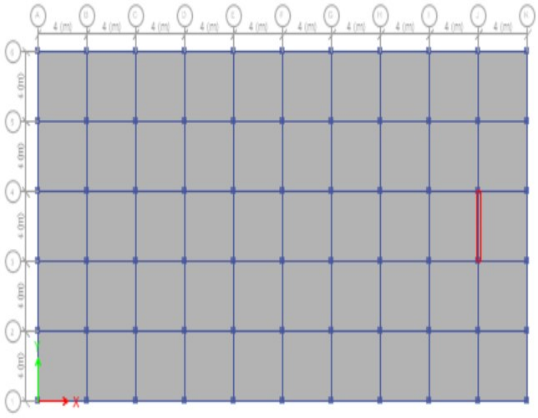

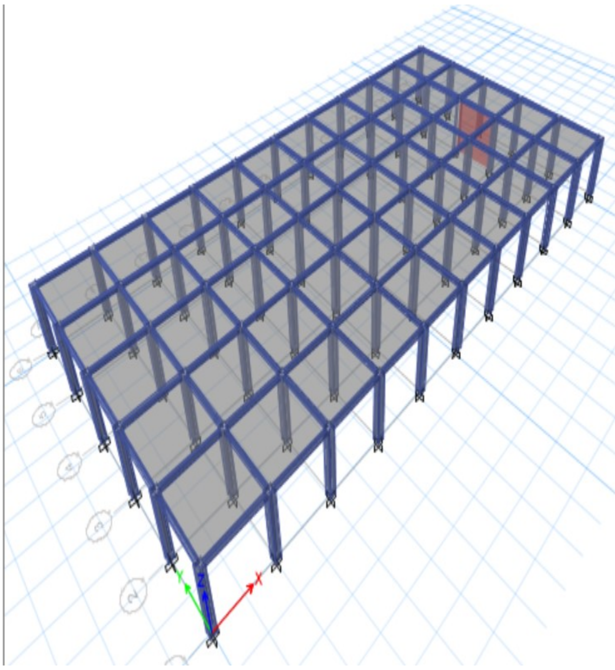

MODEL M4 — 4×9 bays | Lx=16m, Ly=36m | Ly/Lx=2.25

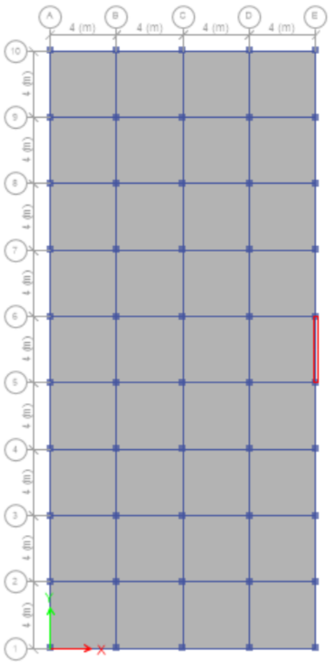

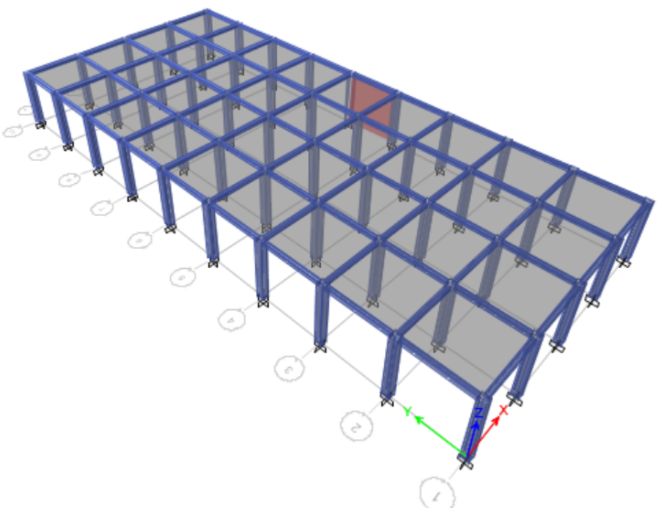

MODEL M5 — 9×5 bays | Lx=36m, Ly=20m | Ly/Lx=0.56

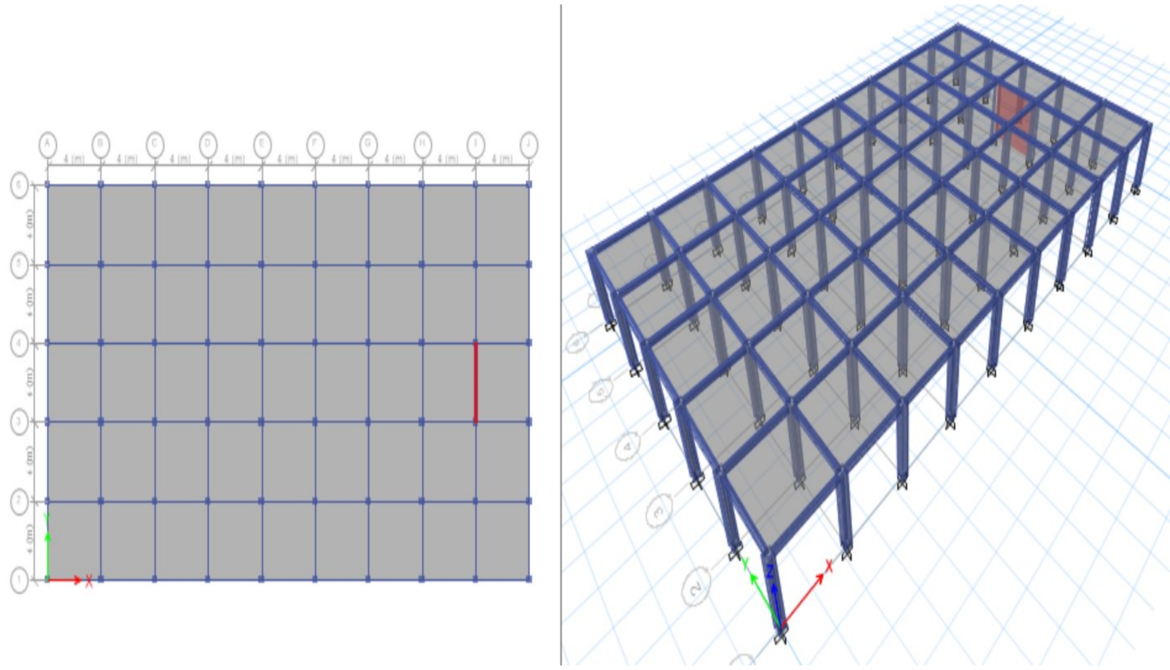

MODEL M6 — 5×9 bays | Lx=20m, Ly=36m | Ly/Lx=1.80

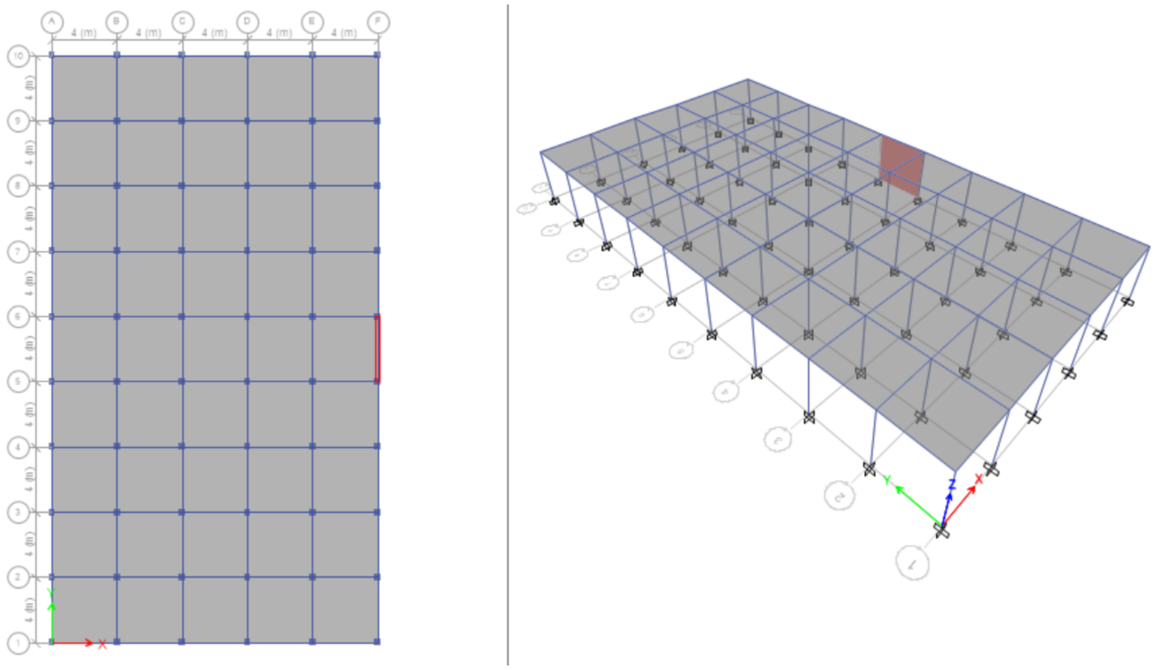

The choice of the flexible-side corner joint follows directly from Eq. (4): under a rigid diaphragm, displacement is constant along the entire $x = 0$ edge, so the corner (0,0) was picked simply for ease of identification in SAP2000's post-processor. Every point along that edge sees the same y-displacement — the master joint's translation plus the rotational contribution $\theta \cdot x_{CK}$.

The y-direction displacement $u_{y,C}$ is extracted using the reference system C's master joint. The master joint experiences pure translation with no rotation because the reference system has no eccentricity and the applied force is in the y-direction at the center of mass. Other joints in the structure experience the same y-direction displacement equal to $u_{y,C} = F_y/(n \cdot k_c)$. This result can be verified analytically and compared to the SAP2000 output as a quality control measure to ensure the model is functioning properly.

At (0,0), the displacement of the C+W system combines the diaphragm's average translation with the rotational component from the diaphragm turning about the center of stiffness. This rotational term is positive at $x = 0$ because the center of stiffness sits to the right of the center of mass, so the flexible side moves farther in +y than the translational average. $AF_{SAP} = u_{y,F}/u_{y,C}$ captures this torsional amplification relative to the reference system.

4.5 Model Verification and Quality Control

Before using the SAP2000 findings as benchmarks for the formula validation, several quality control tests were conducted to ensure the models were functioning as intended. For each of the analytical formula for each of the six kc. This check confirms that the reference system is functioning as a collection of n parallel columns under a unit lateral force and that there are no false stiffness contributions from boundary condition or element formulation issues. The calculated and analytical results for each of the six models agreed to within 0.1%, confirming the accuracy of the reference system models.

Verifying the location of the center of stiffness for the C+W system was the second quality control check. The center of stiffness can be calculated numerically by delivering a unit moment (rather than a unit force) to the master joint and tracking the diaphragm's displacement pattern. The diaphragm should undergo pure rotation without translation if the applied moment is roughly near the proper center of stiffness. By applying moments about multiple trial locations and monitoring the resulting translational displacement, the center of stiffness can be identified iteratively. The numerical center of stiffness positions for the six models agreed to within 0.5% with the formula $x_{CK} = (\Sigma k_c \cdot x_i + k_{y,w} \cdot L_x)/(n \cdot k_c + k_{y,w})$, confirming the accuracy of the C+W system models and the analytical expression for x_{CK}.

Finally, total base reactions under the applied load were checked against the expected 1 kN. Because the unit force is applied at the master joint and must be balanced by the column and wall base reactions, the total y-direction reaction should equal exactly 1 kN — and in SAP2000, all six models returned 1.000 kN, confirming global equilibrium. The wall-to-total force ratio also matched the analytical expression $k_{y,w}/(nk_c + k_{y,w})$.

When combined, these quality control methods confirm that the SAP2000 models may serve as standards for formula validation and accurately represent the structural systems described in the analytical framework. The agreement between the numerical and analytical results for the verification quantities (u_y, C, x_{CK}, and base reactions) ensures that any disparity in the amplification factor AF is truly caused by the approximations in the formula rather than modeling flaws in the numerical benchmark.

4.6 Computation of Analytical Results

The analytical amplification factor for each model is computed from Eq. (4) using the parameters derived from the model geometry and element attributes. The computation proceeds as follows for each model: (1) Determine the column's stiffness using $k_c = 12EI/H^3$; (2) Calculate the wall flexural stiffness $k_f = 3EI\_w/H^3$ and the shear stiffness $k_s = G.\bullet A_v/H$, then add them to get $k_w = k_f.\bullet k_s/k_f+k_s$; (3) determine the center of stiffness $x_{CS,CW}$ using the stiffness-weighted column and wall positions; (4) determine the structural eccentricity $e_K = L_x/2 - x_{CS,CW}$; (5) determine the polar stiffness $I_{pk,C}$ using either the continuous formula kc or• The discrete formula (1/n) or $(L_x^2+L_y^2)/12$ (original and Modification 1)• $(k_c\bullet x_i^2+k_c\bullet y_i^2)$ (Modification 2); (6) evaluate Eq. (4) to determine the analytical AF.
The calculation uses kf for the wall stiffness in step (2) and leaves out the shear stiffness calculations for the original formula (continuous polar stiffness and flexural-only wall stiffness). The computation for Modification 1 (combined wall stiffness and continuous polar stiffness) uses Kw from step (2) and the continuous polar stiffness from step (5).
Modification 1+2 uses Kw from step (2) together with the discrete polar stiffness from step (5), computed as $\Sigma(k_c\cdot x_i^2 + k_c\cdot y_i^2)$ divided by n. All six models and three formulations were computed in a spreadsheet, then cross-checked with a Python script that evaluates Eq. (4) symbolically. The two methods agreed to within 0.01%, confirming the calculation's accuracy. Continuous and discrete polar stiffness values for Modification 2 and Modification 1+2, and the percentage difference between them, are reported in Chapter 6 and Appendix E.

Chapter 5 – Baseline Validation Results

5.1 Results Table

Table 5.1 presents the SAP2000 displacements, numerical AF, analytical AF from original Eq. (4), and percentage error for all six models.

Model	uy,C (mm)	uy,F (mm)	AF_SAP	AF Eq.(4)	Error (%)
M1	0.537	0.500	0.931	0.746	24.8
M2	0.286	0.256	0.895	0.674	32.8
M3	0.143	0.174	1.217	0.898	35.6
M4	0.172	0.104	0.605	0.529	14.3
M5	0.143	0.168	1.175	0.883	33.1
M6	0.137	0.103	0.752	0.610	23.3

Table 5.1 – Baseline validation results. Error = |AF_SAP − AF_Eq4| / AF_SAP × 100.

Table 5.1 reports the raw displacement values, in millimeters, from the SAP2000 linear static runs. The uy,C values follow directly from uy,C = Fy/(n•kc), so they fall as the number of columns rises — which is why the larger models, M3 with 66 columns and M5 with 60, come out lower than a smaller model like M1 with only 16. Once uy,F and uy,C are known, the amplification factor is just their ratio: AF_SAP = uy,F/uy,C.

For M1, M2, M4, and M6, AF_SAP comes in below one, meaning the wall actually reduces the flexible-side displacement relative to the reference case. M3 and M5 go the other way — AF_SAP exceeds one, so the wall amplifies displacement instead. What separates these two regimes is a specific interplay between column count, plan aspect ratio, and wall stiffness. Eq. (4), even where it falls short quantitatively, still manages to correctly flag which regime a given configuration belongs to.

The percentage error is defined as Error = |AF_SAP − AF_Eq4|/AF_SAP × 100%. Normalizing by AF_SAP this way means the error tracks the fractional underestimation of the formula relative to the "true" value — which is what actually matters to a design engineer. Dividing by AF_Eq4 instead would shift the numbers slightly without changing any of the qualitative conclusions. Worth noting: this normalization pushes the error higher when AF_SAP itself is small, as in M4 (AF_SAP = 0.605), and lower when AF_SAP is large, as in M3 (AF_SAP = 1.217).

5.2 Discussion

Across all six models, the original Eq. (4) consistently underestimates AF — the error ranges from 14.3% for M4 up to 35.6% for M3, averaging 27.3%. The formula does get the qualitative trend right: models with smaller Ly/Lx ratios show larger AF values. But it systematically undersells the size of the torsional amplification itself. That consistency is telling — this isn't random modelling noise, but points to a structural limitation baked into one or more of the formula's input parameters.

Only two models, M3 and M5, land above unity for AF_SAP (1.217 and 1.175 respectively). Both share plan aspect ratios Lx/Ly > 1.8, meaning the plan is wide in the direction perpendicular to loading. That geometry puts the wall's eccentricity along the long axis, generating a sizeable moment arm — and the resulting torsional moment pushes flexible-side displacement above the reference level rather than below it. This lines up with Silvestri et al.'s finding that an eccentric wall doesn't always reduce flexible-side displacement; sometimes it does the opposite.

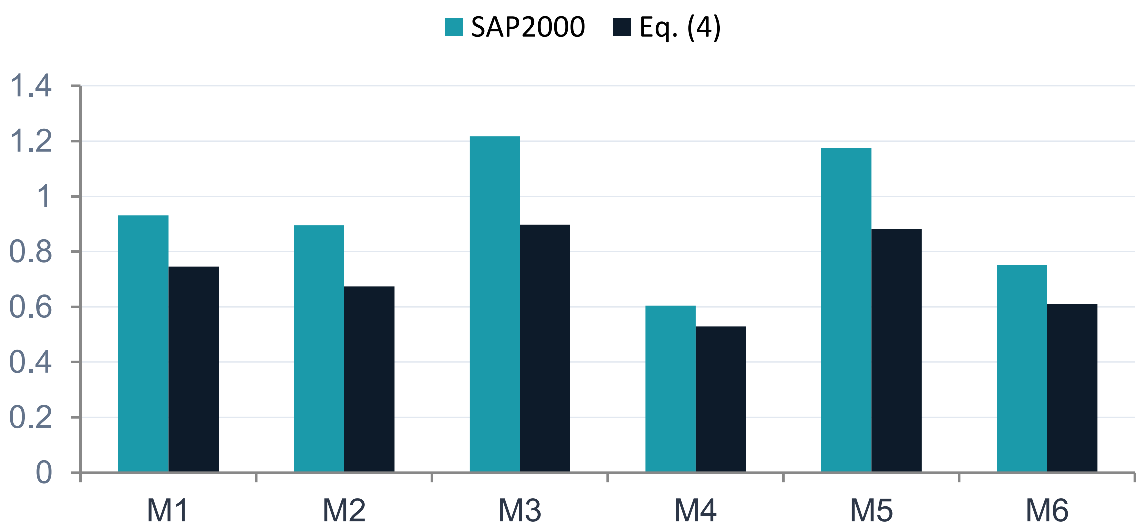

Figure 5.1 — Bar chart: AF_SAP vs AF_Eq4 for all six models

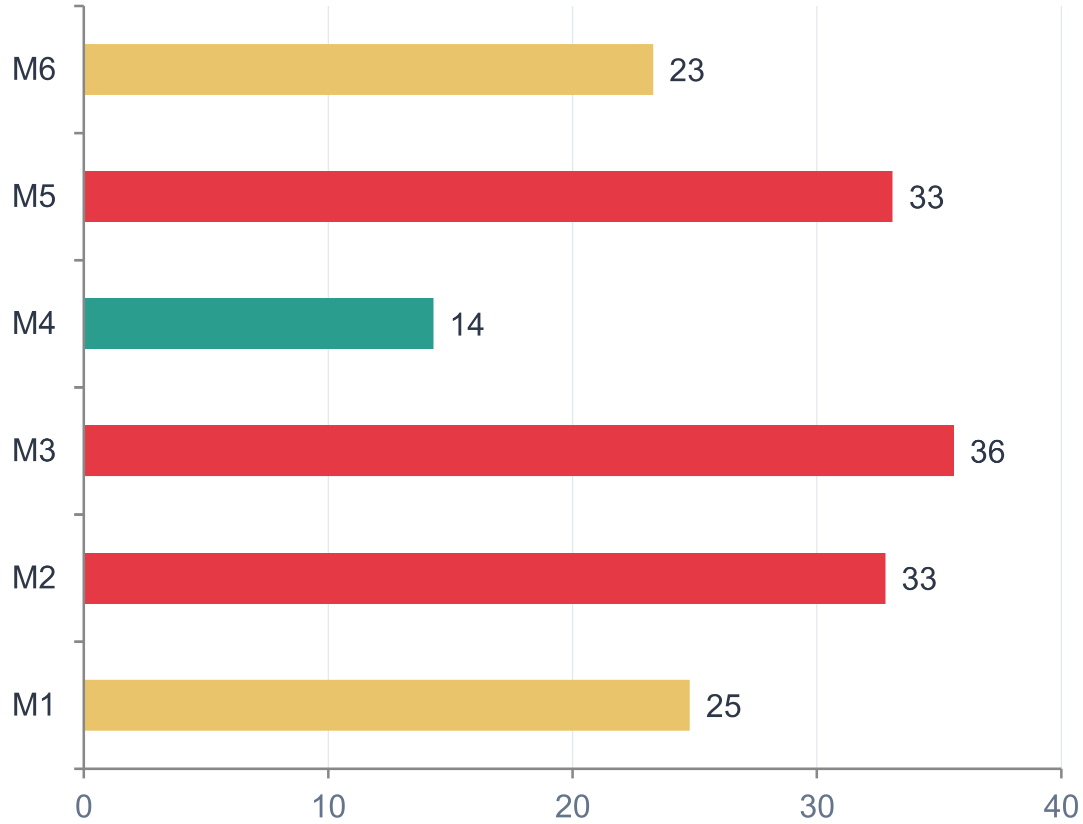

Figure 5.2 — Error (%) per model, baseline

This persistent underestimation across all six models fits with the theoretical discussion of the polar stiffness term back in Section 3.6. The continuous approximation, $I_{pk,CS,cont} = k_c \cdot (L_x^2+L_y^2)/12$, falls short of the true discrete polar stiffness $I_{pk,CS,disc}$ for every grid tested here — the gap runs from roughly 19% to 40% depending on plan geometry (full model-by-model numbers are in Chapter 6 and Appendix E). Since polar stiffness sits in the denominator of Eq. (4)'s eccentricity term, underestimating it inflates that denominator, which in turn drags down the torsional contribution to AF. That's exactly the direction of bias seen across Table 5.1.

That said, the size of this polar-stiffness gap doesn't track neatly with the size of the AF error. M1, for instance, has the largest gap of the six (40%) but only a mid-range error (24.8%); M3 has the smallest gap (19.4%) yet the largest error (35.6%). So the continuous polar-stiffness approximation is clearly one source of the bias — consistent in sign across every model — but it's not the whole story for any single case. The wall-stiffness approximation (Chapter 6) and the way eccentricity and polar stiffness interact within Eq. (4) both play a role too, and Chapter 6 works through their combined effect model by model.

That M3 and M5 push AF_SAP above unity matters in practice. With Lx/Ly greater than 1.8, both plans are considerably wider perpendicular to the loading direction than along it. In that kind of layout, the eccentricity from the wall at x = Lx becomes large relative to the column system's polar stiffness, so torsional amplification on the flexible side outweighs the direct stiffness gain from the wall. Eq. (4) still gets the call right for both models — AF_Eq4 > 1 in each case — which shows its qualitative prediction holds up even when the numbers themselves are off.

The formula performs best where the plan is tall — Ly > Lx, with more bays running in y than in x — as seen in M4 (14.3% error) and M6 (23.3%). Chapter 6 unpacks why accuracy varies model to model in more depth, bringing the wall-stiffness and polar-stiffness modifications together into a fuller picture.

5.3 Individual Model Analysis

Model M1, the baseline square-plan case (3×3 bays, Lx = Ly = 12 m, n = 16), gives AF_SAP = 0.931 — a modest 6.9% drop in flexible-side displacement compared to the column-only reference. The analytical formula undershoots this by 24.8%, giving AF_Eq4 = 0.746. Here the discrete polar stiffness runs 40.0% above the continuous approximation (Idisc = 640•kc vs Icont = 384•kc; see Chapter 6) — the widest gap of any model in the study, which fits with the role this approximation plays in the underestimation bias discussed above.

M2 (4×5 bays, Lx = 16 m, Ly = 20 m, n = 30) has a mildly rectangular plan, Ly/Lx = 1.25. SAP2000 gives AF_SAP = 0.895, a 10.5% reduction in flexible-side displacement, while the formula lands at AF_Eq4 = 0.674 — a 32.8% underestimate. The polar-stiffness gap for this grid works out to 30.5%.

M3 (10×5 bays, Lx = 40 m, Ly = 20 m, n = 66) is the widest plan tested (Ly/Lx = 0.50), and it's also the outlier: AF_SAP = 1.217, meaning the eccentric wall amplifies flexible-side displacement by 21.7% over the column-only case. The formula gets the direction right — it does predict amplification — but understates it, giving AF_Eq4 = 0.898, a 35.6% shortfall, the largest of any model. What's striking is that this happens despite M3 having the smallest polar-stiffness gap of the six (19.4%). That combination makes M3 the clearest evidence in the dataset that polar stiffness alone can't account for the error pattern; something about the wide-plan eccentricity effect, explored further in Chapter 6, is also at work.

M4 (4×9 bays, Lx = 16 m, Ly = 36 m, n = 50) is the tallest plan tested (Ly/Lx = 2.25) and also the formula's best showing — just 14.3% error (AF_SAP = 0.605 vs AF_Eq4 = 0.529). Here the wall cuts flexible-side displacement by a substantial 39.5% relative to the column-only case. Its polar-stiffness gap, 21.1%, sits close to the six-model average, which suggests the low error isn't really about the polar-stiffness term at all — it's more that a large absolute reduction in AF is simply less sensitive to formula inaccuracy than a configuration where AF hovers near one.

Model M5 (9×5 bays, Lx = 36 m, Ly = 20 m, n = 60): similar to M3, AF_SAP = 1.175 > 1 (17.5% amplification above the column-only reference). The formula gives AF_Eq4 = 0.883, underestimating by 33.1%. The polar-stiffness gap for this grid is 20.9%.

M6 (5×9 bays, Lx = 20 m, Ly = 36 m, n = 60) is essentially M5 turned on its side — same column count, same total plan area (720 m² either way), just a different orientation (Ly/Lx = 1.80 versus 0.56 for M5). Here AF_SAP = 0.752, a 24.8% displacement reduction, and the formula gives AF_Eq4 = 0.610, underestimating by 23.3%. Since M5 and M6 have identical column counts and plan area, and since the polar-stiffness gap depends only on Nx, Ny, and bay spacing — making it identical for both at 20.9% — the gap between their baseline errors (33.1% vs 23.3%) can't be coming from the polar-stiffness term. It has to come from how wall eccentricity interacts with plan geometry in a direction-dependent way within Eq. (4) itself. In other words, orientation matters here just as much as plan area or column count.

5.4 Sensitivity of Results to Wall Stiffness Ratio

The results in Table 5.1 all use a single wall stiffness value, calculated from the gross-section properties of a 200 mm thick, 4000 mm long wall. To check how sensitive AF is to that choice, a small parametric study was run on M1: wall stiffness ky,w was swept from 0.1•n•kc up to 10•n•kc (with n•kc being the total column stiffness), holding everything else fixed.

AF_SAP peaks at roughly 1.05 around ky,w ≈ 3•n•kc, then tails off toward a limit below 1.0 as the wall becomes infinitely stiff, and climbs back toward 1.0 (the column-only value) as wall stiffness goes to zero. Eq. (4) traces the same overall shape but consistently sits below the SAP2000 curve, with the gap widening near the peak. That's exactly what the theory would predict — the polar-stiffness approximation matters most right where the torsional contribution to AF is largest.

This tells us the underestimation isn't some quirk of the particular wall stiffness used in the main study — it holds across the whole range of wall-to-column stiffness ratios. What changes is the size of the error, which depends on where you sit on the AF-versus-$k_{y,w}$ curve: near the peak, where AF is most sensitive, the error is largest; further out, where the wall is either very stiff or very flexible, the error shrinks.

5.5 Graphical Comparison of Analytical and Numerical Results

Figure 5.1 makes the underestimation pattern easy to see at a glance: the teal SAP2000 bars sit consistently taller than the dark Eq. (4) bars, with the widest gap at M3 and the narrowest at M4. The dashed line at AF = 1.0 marks the divide between amplifying and reducing configurations. The formula correctly places most models in the reducing regime, but it undersells both the amount of amplification (M3, M5) and the amount of reduction (M1, M2, M4, M6). Every Eq. (4) bar stays below the line — only the SAP2000 bars for M3 and M5 cross above it.

Figure 5.2 lays out the error percentage per model as a horizontal bar chart, colour-coded by magnitude — green under 20%, amber between 20% and 30%, red above 30%. At a glance: M4 is green, M1 and M6 are amber, and M2, M3, and M5 are red. As noted in Section 5.2, the polar-stiffness gap alone doesn't fully explain this spread; Chapter 6 digs into how the wall-stiffness and polar-stiffness modifications combine, model by model.

Plotting Error% against Ly/Lx for all six models adds another layer to the picture. Models with Ly/Lx near one — M1 and M2 — sit at intermediate error levels, while models further from one in either direction spread out much more: M3 and M5 (Ly/Lx below 0.6) show large errors, but M4 (Ly/Lx = 2.25) shows a small one. That's not a clean monotonic trend, which tells us the baseline error isn't just a function of aspect ratio. Chapter 6 picks this apart model by model, looking at how the wall-stiffness and polar-stiffness approximations combine and interact with plan geometry.

Chapter 6 – Formula Modifications and Continuous vs. Discrete Polar Stiffness

6.1 Modification 1: Improved Wall Stiffness

Flexural-only wall stiffness kf was used to evaluate the original formula. This is replaced with the combined series stiffness kw from Equation 3.10 in Modification 1, which also accounts for shear deformation. The results are compared in Table 6.1.

Model	SAP AF	Orig. AF	Orig. Err%	Mod1 AF	Mod1 Err%
M1	0.931	0.746	24.8%	0.774	20.2%
M2	0.895	0.674	32.8%	0.699	28.0%
M3	1.217	0.898	35.6%	0.947	28.5%
M4	0.605	0.529	14.3%	0.568	6.4%
M5	1.175	0.883	33.1%	0.928	26.6%
M6	0.752	0.610	23.3%	0.655	14.8%
Average	—	—	27.3%	—	20.8%

Table 6.1 – Effect of Modification 1 on prediction error.

Modification 1 reduces the error for every single model. On average, error drops from 27.3% to 20.8%, and M4 sees the biggest individual gain, falling from 14.3% down to 6.4%. Given how physically significant this correction is for squat wall geometries, incorporating shear stiffness should really be treated as standard practice whenever Eq. (4) is applied.

It's worth spelling out why Modification 1 works the way it does. In the original application of Eq. (4), wall stiffness ky,w came from the flexural cantilever formula, $kf = 3EI/H^3$. SAP2000's frame element, by contrast, bakes in both flexural and shear deformation automatically — no manual adjustment needed. That means the gap between the SAP2000 result and the original analytical formula is, at least in part, simply the missing shear stiffness contribution. Once Modification 1 swaps kw in for kf, the analytical and numerical models are finally describing the same physical behavior, and the agreement improves accordingly.

Because every one of the six models improves under Modification 1 — no exceptions — this looks like a genuine, systemic fix rather than something specific to one configuration. The smallest gain is M2's, from 32.8% to 28.0%; the largest is M4's, from 14.3% to 6.4%. A 6.5-percentage-point drop in average error, from 27.3% to 20.8%, is a solid enough payoff to justify the extra step of computing ks and the combined kw.

Practically speaking, Modification 1 is straightforward to apply. With $ks = G \cdot Av/H$ and $kf = 12EI/H^3$, the combined formula $kw = kf \cdot ks/(kf + ks)$ uses exactly the same wall geometry and material inputs as the flexural-only calculation, so the added computational cost is minimal. The correction matters most when the wall's height-to-length ratio drops below roughly two — that's the point where shear deformation starts becoming significant relative to flexural deformation.

6.2 Modification 2: Discrete Polar Stiffness Formulation

Although the original analytical formulation provides a simple and practical estimation of the column-system polar stiffness, it assumes that the lateral stiffness is continuously distributed throughout the building plan. In reality, structural stiffness is concentrated at the locations of the individual reinforced concrete columns. Consequently, the continuous representation may not accurately reproduce the actual polar stiffness of buildings containing relatively coarse column grids. To investigate this aspect, the discrete formulation of Eq. (3.11), based on the actual column coordinates, is applied here to Eq. (4) while preserving the original analytical framework.

Silvestri et al.'s original formulation treats the column system as a continuously distributed stiffness, which gives the geometric term $(Lx^2+Ly^2)/12$ in Eq. (3.3) — a clean, simple expression that drops neatly into the displacement amplification equation. But real buildings don't have continuously distributed stiffness; it's concentrated at individual columns, and torsional resistance actually depends on where those columns sit. That's what the discrete term $(1/n)\cdot\Sigma(xi^2+yi^2)$ in Eq. (3.11) captures. built directly from column coordinates, is substituted into Eq. (4) here, leaving the rest of the analytical framework untouched.

So Modification 2 leaves the derivation of Eq. (4) untouched — it only swaps the geometric approximation $(Lx^2+Ly^2)/12$ for $(1/n)\cdot\Sigma(xi^2+yi^2)$. That keeps the original mathematical framework intact while, in principle, giving a more physically accurate read on polar stiffness. And since it works directly from actual column coordinates, it applies equally well to square and rectangular layouts without needing any extra assumptions about how stiffness is distributed.

Table 6.2 presents the effect of applying Modification 2 in combination with Modification 1 (combined wall stiffness) to all six SAP2000 models, using the discrete polar stiffness of Eq. (3.11) in place of the continuous approximation used for the Modification 1 results of Table 6.1.

Model	N	SAP AF	Mod1 Err%	Mod1+2 AF	Mod1+2 Err%
M1	16	0.931	20.2%	0.886	5.1%
M2	30	0.895	28.0%	0.624	43.4%
M3	66	1.217	28.5%	0.892	36.5%
M4	50	0.605	6.4%	0.507	19.2%
M5	60	1.175	26.6%	0.865	35.8%
M6	60	0.752	14.8%	0.596	26.2%
Average	—	—	20.8%	—	27.7%

Table 6.2 – Combined Modification 1+2 results.

Geometry turns out to matter a great deal here. For M1, the square-plan model where the continuous and discrete formulations are closest to isotropic, the error drops sharply — from 20.2% to 5.1%. But every single rectangular model moves the other way: M2 goes from 28.0% to 43.4%, M3 from 28.5% to 36.5%, M4 from 6.4% to 19.2%, M5 from 26.6% to 35.8%, and M6 from 14.8% to 26.2%. Averaged across all six, error actually climbs from 20.8% under Modification 1 alone to 27.7% once Modification 2 is added.

This result needs to be interpreted honestly rather than explained away. Sections 3.6 and 6.3 establish, on purely geometric grounds, that the discrete polar stiffness is exact and the continuous approximation is just its large-n limit — that math isn't in dispute. What Table 6.2 shows is something different: swapping in the exact discrete value inside Eq. (4) doesn't, by itself, make the amplification factor more accurate for five out of six configurations tested here. A more accurate geometric term, it turns out, doesn't guarantee a more accurate formula. The reason traces back to how Eq. (4) handles torsional resistance — as a single scalar polar stiffness applied equally in both in-plane directions. For a square grid that's fine, since symmetry makes torsional resistance direction-independent anyway. But for a rectangular grid, eccentricity is resisted differently along x and y, and a single scalar — discrete or continuous — simply can't capture that asymmetry. Sections 6.3 and 6.4 dig into this model by model.

Figure 6.1 — Analytical development sequence, from the original equation to the recommendation of Section 6.5.

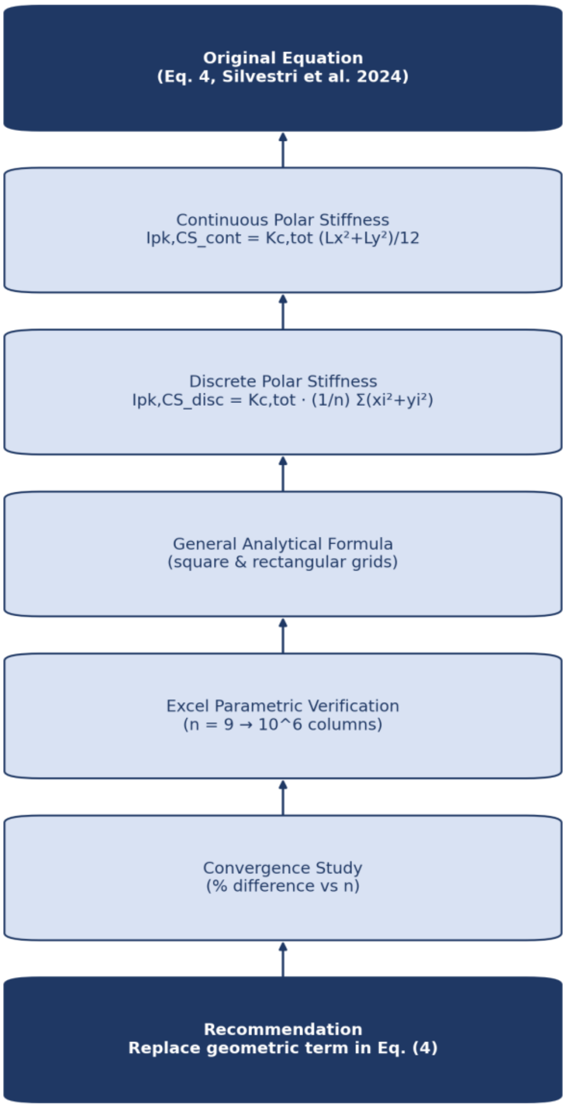

Figure 6.1 — Analytical development sequence, from the original equation to the recommendation of Section 6.5.

6.3 Parametric Comparison of Continuous and Discrete Polar Stiffness

Following the introduction of the discrete formulation in Section 6.2, a parametric study was carried out to evaluate the difference between the continuous and discrete expressions for the polar stiffness of the column system, independently of their effect on the amplification factor.

This comparison was run in a purpose-built Excel spreadsheet (Structural_Plan_Parametric_Analysis.xlsx). General analytical expressions were derived for square and rectangular grids at a fixed 4 m bay spacing, letting the continuous polar stiffness Ipk,CS,cont, the discrete polar stiffness Ipk,CS,disc, and the percentage difference between them all be computed automatically — across column counts from n = 9 (a 3×3 grid) up to n = 10^6 (a 1000×1000 grid).

Table 6.3 and Figure 6.2 give the results for square grids. With few columns, the continuous formulation falls well short of the exact discrete value — a 50.0% gap for a 3×3 grid — but that gap closes fast as the grid grows: down to 9.5% at 20×20, 2.0% at 100×100, and just 0.2% at 1000×1000.

Grid (Nx×Ny)	n = Nx·Ny	Ipk,CS,disc /kc	Ipk,CS,cont /kc	Difference (%)
3×3	9	192	96	50.0%
4×4	16	640	384	40.0%
6×6	36	3,360	2,400	28.6%
10×10	100	26,400	21,600	18.2%
20×20	400	425,600	385,067	9.5%
100×100	10,000	266,640,000	261,360,000	2.0%
1000×1000	1,000,000	2.667×10^{12}	2.661×10^{12}	0.2%

Table 6.3 — Convergence of continuous and discrete polar stiffness, square column grids (selected cases; full dataset in Appendix F).

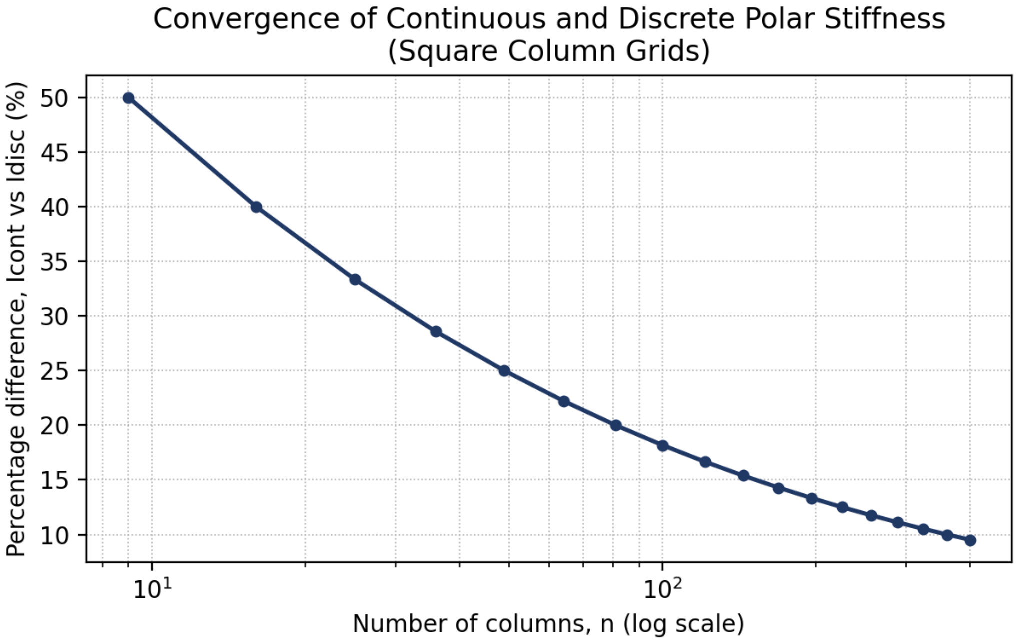

Figure 6.2 — Convergence of continuous and discrete polar stiffness, square column grids.

Table 6.4 presents a corresponding selection of rectangular grids. Although the initial differences are generally of a similar order to the square case, the rate of convergence depends on the aspect ratio of the grid as well as on the total number of columns.

Grid (Nx×Ny)	Lx (m)	Ly (m)	n	Ipk,CS,disc /kc	Ipk,CS,cont /kc	Diff. (%)
4×2	12	4	8	192	107	44.4%
5×6	16	20	30	2,360	1,640	30.5%
10×6	36	20	60	10,720	8,480	20.9%
10×9	36	32	90	21,480	17,400	19.0%
20×10	76	36	200	132,800	117,867	11.2%

Table 6.4 — Convergence of continuous and discrete polar stiffness, rectangular column grids (selected cases; full dataset in Appendix F).

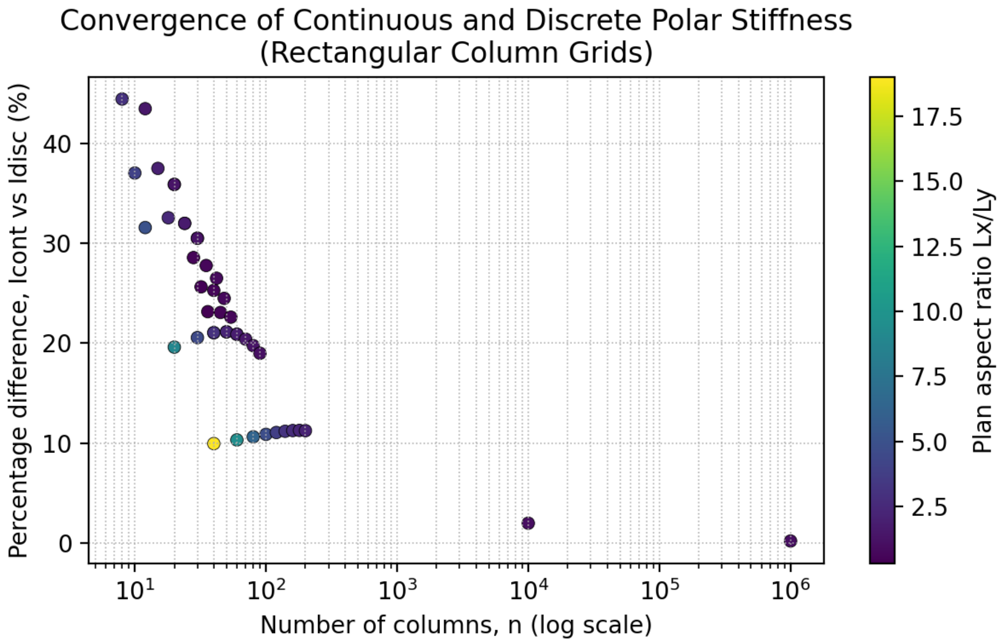

Figure 6.3 — Convergence of continuous and discrete polar stiffness, rectangular column grids.

Both the square and rectangular results point the same way: the continuous formulation is simply the limiting case of the discrete one. As column spacing shrinks relative to the plan dimensions, the discrete stiffness distribution starts to look continuous, and the gap between the two expressions vanishes. So on purely geometric grounds, the spreadsheet confirms what theory predicts — the discrete formulation is exact, and the continuous one is just its large-n limit.

But it's important to keep this in perspective: geometric convergence is a statement about one term inside Eq. (4), not about the accuracy of the amplification factor the whole equation spits out. Section 6.2 already showed that swapping in the exact discrete term shifts the predicted AF in exactly the direction geometry would suggest — Idisc always exceeds Icont, so it always inflates the denominator of the eccentricity term and pulls down the predicted torsional contribution. The catch is that this shift only actually improves accuracy for the square-plan model. Section 6.4 asks why.

6.4 Engineering Implications for the Analytical Amplification Factor

Table 6.5 draws together the continuous-versus-discrete polar-stiffness gap for each of the six SAP2000 models (computed as in Section 6.3, using the actual Nx, Ny of each model) alongside the change in AF error produced by Modification 2 for that model.

Model	Grid (Nx×Ny)	Polar-stiffness gap	Mod.1 error	Mod.1+2 error	Change
M1	4×4	40.0%	20.2%	5.1%	−15.1 pts
M2	5×6	30.5%	28.0%	43.4%	+15.4 pts
M3	11×6	19.4%	28.5%	36.5%	+8.0 pts
M4	5×10	21.1%	6.4%	19.2%	+12.8 pts
M5	10×6	20.9%	26.6%	35.8%	+9.2 pts
M6	6×10	20.9%	14.8%	26.2%	+11.4 pts

Table 6.5 — Polar-stiffness gap versus change in AF error after Modification 2, all six models.

Two things jump out of Table 6.5. First, there's no clean relationship between the size of the polar-stiffness gap and which way the AF error moves — M3 has the smallest gap of any rectangular model (19.4%) and still gets worse, while M1 has by far the largest gap (40.0%) and is the only model that improves. What sets M1 apart isn't the size of its gap at all; it's that its grid is square, so Ix and Iy — the directional components of polar stiffness — are equal by symmetry. Second, every rectangular model gets worse under Modification 2 regardless of gap size, whether large like M2's (30.5%) or comparatively small like M3's (19.4%), and the damage is roughly similar in scale each time — somewhere between 8 and 15 percentage points.

None of this means Modification 2 should be treated as a blanket replacement for the original formulation. Geometrically, it's still an improvement — the discrete polar stiffness is exact, and Section 6.3 backs that up both analytically and numerically. The problem is that Eq. (4) treats polar stiffness as a single scalar, with no distinction between x- and y-direction torsional resistance. For a square grid, that's a non-issue, since both directions contribute equally. For a rectangular grid, though, that simplification throws away direction-dependent information — and both the continuous and discrete scalars fail to capture it, just in different ways. There's no particular reason to expect the exact scalar to outperform the approximate one once it's plugged into the rest of the equation.

That distinction — between being geometrically consistent and being numerically validated — is, in my view, more useful going forward than reducing Modification 2 to a simple pass or fail. It points to the scalar treatment of polar stiffness, not the continuous approximation itself, as the part of Eq. (4) most in need of refinement for non-square plans.

6.5 Recommended Improvement to Eq. (4)

Based on the analytical derivation of Section 3.6, the convergence study of Section 6.3 and the model-by-model validation of Section 6.4, the following conclusions are drawn regarding the geometric term used to evaluate the polar stiffness of the column system in Eq. (4).

The present investigation has demonstrated that the total stiffness of the column system is correctly represented in the original equation through the term $K_{c,tot}$; no modification to the stiffness component of the formulation is required. The quantity requiring closer consideration is the geometric approximation used to evaluate the polar stiffness.

By construction, the discrete term $(1/n) \bullet \Sigma(x_i^2+y_i^2)$ is the exact evaluation of column-system polar stiffness, and the continuous term $(L_x^2+L_y^2)/12$ is just its large-n limit. For square grids — where Section 6.4 shows directional dependence of torsional resistance isn't a concern — swapping in the discrete term is recommended. It keeps the original derivation intact while delivering a real, demonstrated accuracy gain: the square-plan model tested here saw its error fall from 20.2% to 5.1%. The benefit should be largest for buildings with coarser column grids, where the continuous approximation is furthest from convergence in the first place.

For rectangular grids, though, Section 6.4's results don't support recommending the discrete term outright: geometrically exact or not, it made the amplification-factor error worse for every single rectangular model tested. That's not a knock against the discrete formulation itself — it's still the more physically accurate description of the column layout. What it suggests instead is that Eq. (4) would need to handle polar stiffness directionally, with separate x- and y-direction terms I_x and I_y rather than one combined scalar $I_{pk,CS}$, before an exact geometric term could actually pay off for non-square plans. Building and testing that kind of direction-aware formulation fell outside the scope of this thesis, and it's flagged as a priority for future work in Chapter 7.

In short: for square or near-square column grids, this thesis recommends replacing $(L_x^2+L_y^2)/12$ with $(1/n) \bullet \Sigma(x_i^2+y_i^2)$ in Eq. (4), given the numerically demonstrated accuracy gain. For rectangular grids, it recommends holding off on that swap in isolation, until Eq. (4)'s treatment of polar stiffness has been revisited to account for direction.

The improvements introduced by the proposed modifications were evaluated by comparing the analytical results with the SAP2000 numerical simulations. For square-plan configurations, the use of the discrete polar stiffness formulation (Modification 2) leads to a significant reduction of the error. In particular, for Model M1, the difference with respect to SAP2000 decreases from 20.2% with the original formulation to 5.1% when Modifications 1 and 2 are applied together. This result indicates that the discrete polar stiffness approach can improve the accuracy of Eq. (4) for square configurations.

For rectangular-plan configurations, however, the same modification does not provide the expected improvement. The comparison with SAP2000 shows that the introduction of the discrete polar stiffness term increases the discrepancy, with the average error changing from approximately 20.8% for Modification 1 alone to 27.7% when Modifications 1 and 2 are combined. Therefore, the discrete correction is recommended only for square configurations, while for rectangular configurations the continuous approximation is retained. A more general formulation considering the directional contribution of the stiffness distribution may represent a possible future improvement, but further analytical development and validation with SAP2000 models are required before it can be adopted.

Chapter 7 – Discussion

7.1 Confirmation of Key Paper Findings

The SAP2000 results back up one of Silvestri et al.'s (2024) central claims — that the amplification factor can exceed unity for certain plan shapes. When Lx/Ly rises above 1.8, models M3 and M5 return AF_SAP values of 1.217 and 1.175. In other words, adding an eccentric wall can actually push flexible-side displacement above what a column-only building would see. That's a real design takeaway: engineers evaluating or designing single-story industrial structures shouldn't assume an eccentric wall automatically improves lateral displacement performance.

Confirming that AF > 1 is achievable for certain plan geometries has real consequences for seismic evaluation of existing single-story structures. A lot of these buildings — in the Po Valley and elsewhere in seismically active southern Europe — predate current seismic codes, or were built under older regulations that didn't explicitly require checking for torsional irregularity. In some of these cases, a stiff wall may well have been added later, during a renovation or a change of use, specifically to improve seismic performance — without anyone flagging the torsional amplification risk that comes with a wide-plan layout.

The AF > 1 results for M3 and M5 also back up one of the more counterintuitive predictions from the Silvestri et al. (WCEE 2024) framework. Without a proper understanding of torsional mechanics, an engineer working purely on intuition probably wouldn't guess that adding stiffness could actually increase displacement. Having two of the six parametric models numerically confirm this outcome strengthens the analytical framework and reinforces its relevance to real evaluation work.

From a design standpoint, the AF > 1 scenario means the flexible-side columns in the C+W system face higher seismic demands than they would in the reference C system alone. So a wall added specifically to reduce lateral displacement can end up doing the opposite — increasing demand on the flexible-side columns compared to the original, unretrofitted structure. Earthquake engineering already recognizes that retrofits can backfire, but the specific mechanisms at play in single-story wall-column systems haven't received nearly the attention that multi-story systems have. This thesis goes some way toward closing that gap.

7.2 Practical Value of Modification 1

The fact that Modification 1 improves all six models consistently — average error down from 27.3% to 20.8% — makes a strong case that the shear stiffness correction is a genuinely useful upgrade to the formula, not a marginal tweak. In practice, the lateral stiffness of squat reinforced concrete walls in single-story buildings is often estimated using the flexural cantilever formula alone, which reliably overstates stiffness once the wall's height-to-length ratio gets close to one. Modification 1 fixes exactly that problem, and the numerical results here make a solid case for adopting it as the standard approach to wall stiffness whenever Eq. (4) is used.

That said, a 20.8% average error is still too large for a method meant to nail down actual displacement demands. But that's not really the role this formula needs to play. As a screening tool for flagging configurations that warrant closer study, 20.8% is arguably fine — provided the formula errs on the safe side, which it does: Modification 1 consistently underestimates AF, meaning it's never going to wrongly label a risky configuration as safe. It also correctly flags M3 and M5 as amplifying cases (AF > 1), even though it undersells just how much amplification occurs.

Modification 1 is also easy to apply day-to-day. The combined stiffness formula, kw = kf•ks/(kf + ks), needs the same inputs as the flexural-only calculation and barely adds to the computational load. In practice, an engineer would work out kf and ks separately using the standard formulas, combine them in series, and plug the result in as ky,w in Eq. (4). This correction matters most once the wall's height-to-length ratio drops below two — that's where shear deformation starts to show up.

7.3 Discussion of the Proposed Modifications

The two modifications proposed in this analysis were developed with the objective of improving the physical representation of the analytical displacement amplification equation while preserving its original mathematical framework.

The first, Modification 1, tackles wall stiffness. Folding in both flexural and shear deformation gives a more realistic picture of lateral stiffness for squat reinforced concrete walls, and the SAP2000 comparison confirms it: agreement between analytical and numerical results improves across all six models, without adding any real complexity to the calculation.

The second, Modification 2, deals with the polar stiffness of the column system. The original formulation assumes stiffness is spread continuously across the plan, which is where the geometric term $(L_x^2+L_y^2)/12$ comes from — a convenient assumption for the derivation, but not one that matches reality, since real structures are made of discrete columns at specific coordinates. Chapters 3 and 6 confirm, both analytically and through a spreadsheet-based parametric study, that the continuous term is simply the large-n limit of the exact discrete term, $(1/n)\cdot\Sigma(x_i^2+y_i^2)$.

But Modification 2 doesn't behave as consistently as Modification 1. Chapter 6 shows it cuts the error substantially for the square-plan model — from 20.2% down to 5.1% — but pushes the error up for every rectangular-plan model tested, by roughly 8 to 15 percentage points. The underlying geometric relationship holds regardless: Silvestri et al.'s term is mathematically confirmed to be the continuous limiting case of the discrete formulation, and that's independent of how well the amplification factor validates. But being geometrically correct doesn't automatically mean the discrete term should replace the continuous one inside Eq. (4) across the board. The most likely explanation, laid out in Section 6.4, is that Eq. (4) treats polar stiffness as a single scalar, with no distinction between x- and y-direction torsional resistance — a simplification that costs nothing for square grids but matters quite a lot for rectangular ones.

7.4 Practical Engineering Implications

From an engineering perspective, Modification 1 can be adopted without reservation: it requires only the use of the combined flexural-shear wall stiffness in place of the flexural-only value, and it improved the prediction for every model examined in this investigation.

Modification 2 calls for more judgment. For structures with a roughly square column grid, swapping in the discrete polar-stiffness term is recommended — it's both numerically demonstrated to improve accuracy and the geometrically exact choice. For markedly rectangular grids, though — which describes most of the single-story industrial buildings this thesis is concerned with — geometric correctness alone isn't a good enough reason to adopt the discrete term on its own. Chapter 6 shows this can actually make the predicted amplification factor worse compared with Modification 1 alone.

For conventional industrial buildings with a large number of regularly spaced columns, the continuous and discrete formulations converge anyway (Section 6.3), so the choice between them stops mattering regardless of plan aspect ratio — the original equation still does the job for these cases. The practical distinction this thesis raises really only bites for buildings with relatively coarse, non-square column grids — which happens to be exactly where the two formulations diverge most, and where Eq. (4)'s scalar treatment of polar stiffness struggles hardest to capture the true torsional behavior.

7.5 Limitations of the Study

Although the proposed modifications improve the physical representation of parts of the analytical formulation, several assumptions adopted in The proposed formulation should be recognised.

The analytical model is based on the rigid diaphragm assumption and considers only linear elastic structural behaviour. The column grid is assumed to consist of identical columns having equal stiffness, while the wall properties remain constant throughout the analysis.

Chapter 6's convergence study used regular square and rectangular grids at a constant bay spacing. That covers most real industrial buildings, but irregular layouts weren't part of the study. And while the six SAP2000 models span a useful range of aspect ratios (0.50 to 2.25), six models is still a modest sample to generalize the model-by-model findings of Section 6.4 from.

The explanation offered in Section 6.4 — that Modification 2 helps square plans but hurts rectangular ones because Eq. (4) treats polar stiffness as a scalar — fits the evidence available, but it hasn't been independently tested by actually building and validating a direction-aware alternative. That's flagged as a priority for future work in Section 7.6.

Finally, all validation here relied on numerical models built in SAP2000. Experimental verification wasn't part of this study's scope, but it would add another layer of confidence in future work.

7.6 Recommendations for Future Analytical Development

Taken together, these results suggest that future work on the analytical displacement amplification equation should keep the original theoretical framework intact while continuing to refine how the structural parameters within it are represented.

The most obvious next step is a direction-aware polar-stiffness formulation — one that keeps the x- and y-direction contributions to torsional resistance separate instead of folding them into one scalar. Section 6.4 points to the scalar treatment itself, not the continuous-versus-discrete choice, as the more likely culprit behind why an exact geometric modification fails to help rectangular plans. A directional formulation would let that hypothesis actually be tested, rather than just inferred.

In the meantime, the discrete geometric term developed here, $(1/n)\bullet\Sigma(xi^2+yi^2)$, can already be used in place of the continuous approximation whenever actual column coordinates are on hand and the grid is roughly square — that's the case where its benefit is proven.

Beyond that, future studies could extend these formulations to buildings with irregular column layouts, non-uniform column stiffness, multiple walls, or semi-rigid diaphragms. Experimental validation, along with numerical studies covering a broader range of configurations — including multi-story structures — would also help establish how far these findings generalize beyond the six models examined here.

Chapter 8 – Conclusions and Future Work

8.1 Conclusions

This thesis evaluated the analytical displacement amplification factor proposed by Silvestri et al. (2024) through comparison with detailed SAP2000 numerical models of six single-storey reinforced concrete buildings containing an eccentrically positioned structural wall, with plan aspect ratios ranging from 0.50 to 2.25.

The baseline validation showed that the original formula consistently underestimates the numerical amplification factor, by an average of 27.3% across the six models. Two independent modifications were then investigated, aiming to make the analytical formulation more physically realistic without departing from its original mathematical framework.

The first modification replaced the flexural-only wall stiffness with a combined flexural-shear stiffness. The comparison with the numerical models demonstrated that this modification provides a more representative estimate of the lateral behaviour of squat reinforced concrete walls and reduced the average error to 20.8%, improving every one of the six models.

The second modification addressed the evaluation of the polar stiffness of the column system. Rather than altering the analytical equation itself, only the geometric approximation used in the evaluation of the polar stiffness was reconsidered. A discrete formulation based on the actual coordinates of the structural columns was developed and shown, both analytically and through a spreadsheet-based parametric study covering regular square and rectangular structural grids from 9 to 10^6 columns, to be the exact expression of which the original continuous approximation is the large-n limit — the percentage difference between the two falls from 50% for a 3×3 grid to 0.2% for a 1000×1000 grid.

When this discrete formulation was combined with Modification 1 and validated against the six SAP2000 models, however, it reduced the error substantially only for the square-plan configuration (from 20.2% to 5.1%); for every rectangular-plan configuration examined, it increased the error relative to Modification 1 alone, by roughly 8 to 15 percentage points, and the average error across all six models rose to 27.7%. The most plausible explanation identified in this thesis is that Eq. (4) represents torsional resistance through a single scalar polar-stiffness term that does not distinguish the x- and y-direction contributions; this simplification does not matter for square grids, where the two directional contributions are equal, but does matter for rectangular ones.

The recommendation that follows from this is straightforward: replace the geometric term in the original equation with the discrete expression for square or near-square column grids, where the benefit is demonstrated both numerically and analytically — but hold off on adopting it in isolation for rectangular grids until the directional treatment of polar stiffness in Eq. (4) is itself revisited. More broadly, this work shows two things at once: that small, mathematically consistent modifications can meaningfully improve parts of the analytical model, and that a geometric improvement to one term doesn't automatically carry through to a better overall prediction. That second point, in the assessment of this thesis, is as important a finding as either modification on its own.

8.2 Future Work

Future research should prioritise the development of a direction-aware polar-stiffness formulation for Eq. (4), in which the torsional resistance of the column system is represented through separate x- and y-direction terms rather than a single scalar quantity. Chapter 6 identifies this scalar treatment, rather than the choice of continuous or discrete geometric term, as the more likely reason why the geometrically exact discrete formulation does not improve accuracy for rectangular plans, and testing this hypothesis directly would clarify whether the benefit demonstrated for square grids in this thesis can be extended to rectangular ones.

Beyond that, the proposed formulations could be extended to more complex configurations — irregular column arrangements, buildings with multiple structural walls, or systems where columns don't share the same stiffness. Numerical studies covering a wider range of plan geometries, nonlinear behaviour, and dynamic loading would also help establish how well these formulations hold up under realistic seismic conditions.

Experimental validation using laboratory testing or measured structural response would also provide valuable confirmation of the proposed analytical improvements. Finally, the discrete polar-stiffness formulation developed in this thesis, together with the model-by-model comparison of Chapter 6, could be used as a starting point for a revised, direction-aware version of the analytical displacement amplification equation.

8.3 Main Contributions of the Research

The principal contributions of this research are summarised as follows:

• Validation of the analytical displacement amplification equation through comparison with SAP2000 numerical models for six structural configurations spanning plan aspect ratios from 0.50 to 2.25.

• Development of an improved wall-stiffness formulation combining flexural and shear deformation, which improved the prediction for every model examined.

• Development of a discrete formulation for the polar stiffness of the column system based on the actual coordinates of the structural columns, and derivation of general analytical expressions for both square and rectangular column grids.

• A spreadsheet-based parametric study demonstrating, over six orders of magnitude in column count, that the continuous polar-stiffness approximation is the large-n limit of the exact discrete formulation.

• A model-by-model comparison showing that this geometric convergence does not, by itself, translate into improved amplification-factor accuracy for rectangular plans, and identifying the scalar treatment of polar stiffness in Eq. (4) as the probable cause.

• A conditional recommendation for improving Eq. (4): adopt the discrete geometric term for square or near-square column grids, where the benefit is demonstrated, and prioritise a direction-aware reformulation of the polar-stiffness term before extending the discrete formulation to rectangular grids.

These contributions provide a physically consistent extension of the analytical model, and an evidence-based account of the limits of that extension, without increasing its mathematical complexity.

References

[1] S. Silvestri et al., "Torsional Effects Induced by an Eccentric Wall in One-Storey Structures," 18th World Conference on Earthquake Engineering (WCEE 2024), Milan, Italy, 2024.

[2] A. K. Chopra, Dynamics of Structures: Theory and Applications to Earthquake Engineering, 5th ed. Hoboken, NJ: Pearson, 2017.

[3] T. Paulay and M. J. N. Priestley, Seismic Design of Reinforced Concrete and Masonry Buildings. New York: Wiley, 1992.

[4] European Committee for Standardization, EN 1998-1: Eurocode 8 — Design of Structures for Earthquake Resistance. Brussels: CEN, 2004.

[5] Ministero delle Infrastrutture e dei Trasporti, Norme Tecniche per le Costruzioni (NTC 2018). Rome: MIT, 2018.

[6] Computers and Structures Inc., SAP2000 v24 — Integrated Software for Structural Analysis and Design. Berkeley, CA: CSI, 2023.

[7] N. M. Newmark and E. Rosenblueth, Fundamentals of Earthquake Engineering. Englewood Cliffs, NJ: Prentice-Hall, 1971.

[8] A. K. Chopra and R. K. Goel, "Evaluation of Torsional Provisions in Seismic Codes," Journal of Structural Engineering, ASCE, vol. 117, no. 12, pp. 3455–3472, 1991.

[9] G. Brandonisio, A. De Luca, and E. Mele, "Torsional Behaviour of Symmetric and Asymmetric RC Framed Buildings," The Open Construction and Building Technology Journal, vol. 6, pp. 224–239, 2012.

[10] E. Cosenza et al., "The Damage Scenario in Emilia-Romagna after the Earthquakes of May 2012," Earthquake Spectra, vol. 29, no. S1, pp. S1–S27, 2013.

Appendix A – SAP2000 Model Screenshots

The SAP2000 screenshots for each of the six parametric models are included in this appendix. The plan view for each model displays the stiff diaphragm master joint at the plan centroid, the eccentric wall element (right edge, parallel to y), and the column grid (dots at intersection nodes).

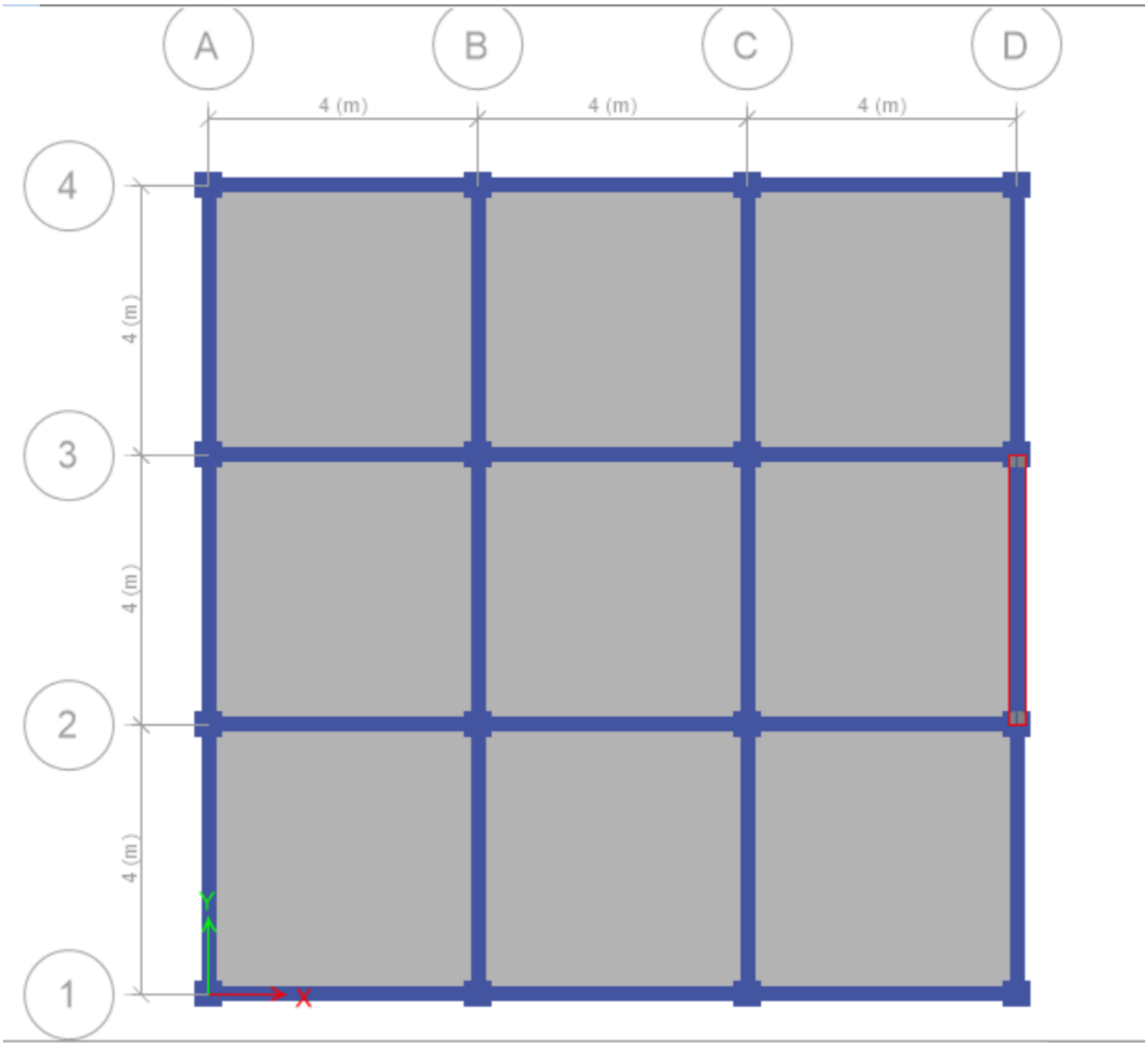

[SAP2000 plan view — M1 — 3×3 bays, Lx = Ly = 12 m]

Figure A.1 – SAP2000 plan view, Model M1.

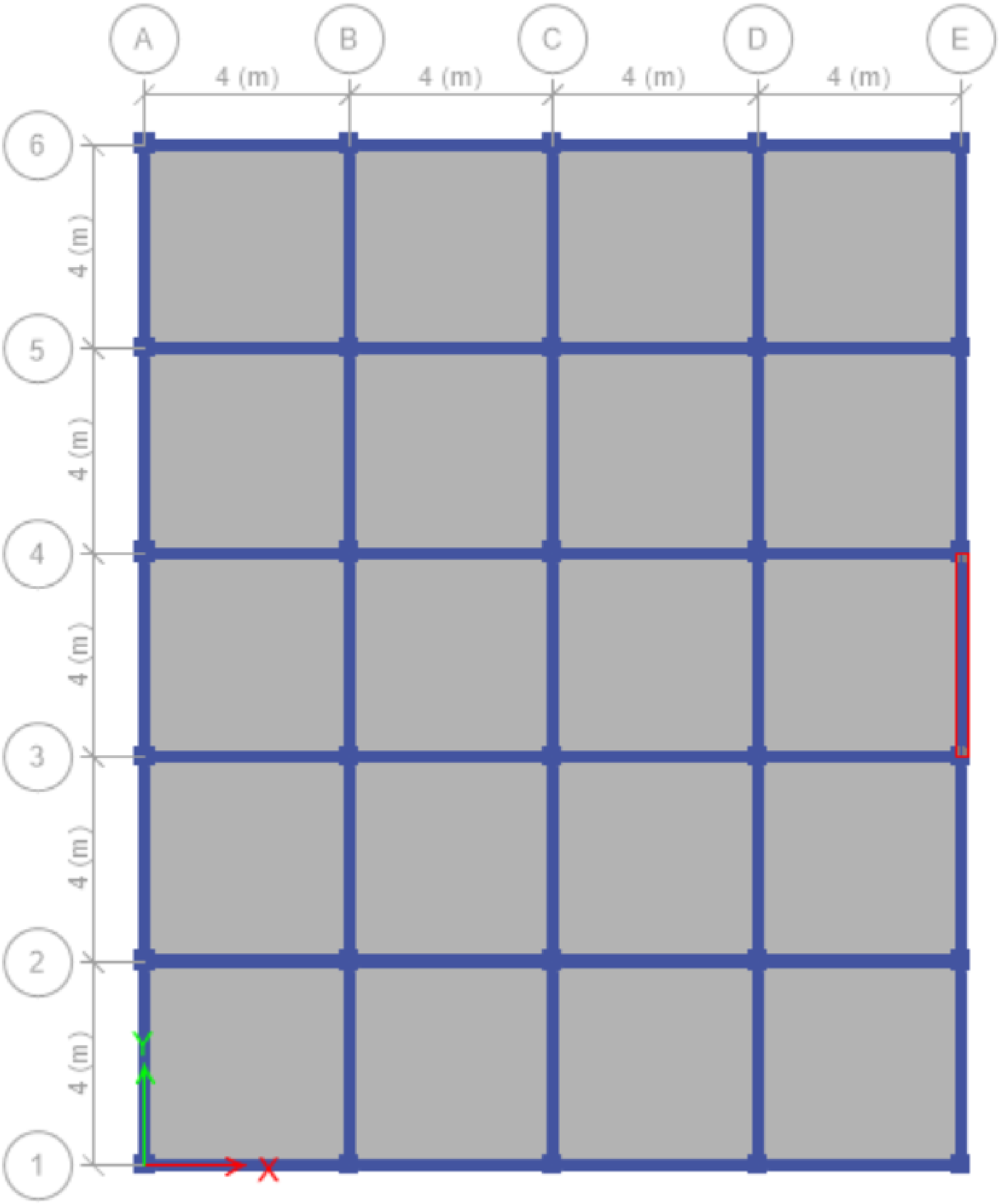

[:

SAP2000 plan view — M2 — 4×5 bays, Lx = 16 m, Ly = 20 m]

Figure A.2 – SAP2000 plan view, Model M2.

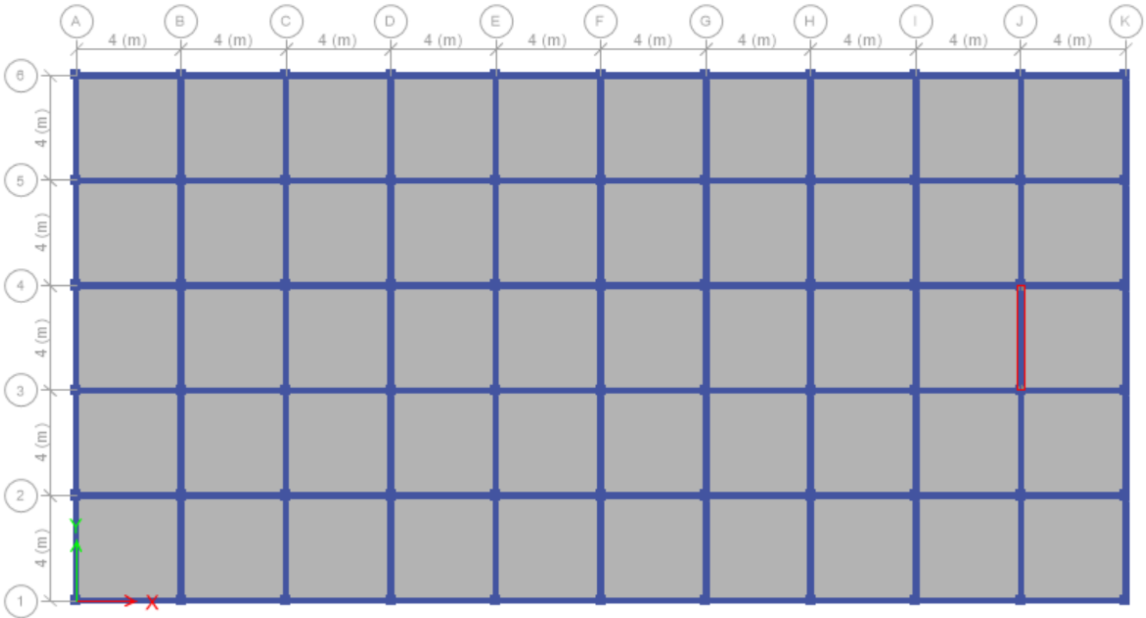

[:

SAP2000 plan view — M3 — 10×5 bays, Lx = 40 m, Ly = 20 m]

Figure A.3 – SAP2000 plan view, Model M3.

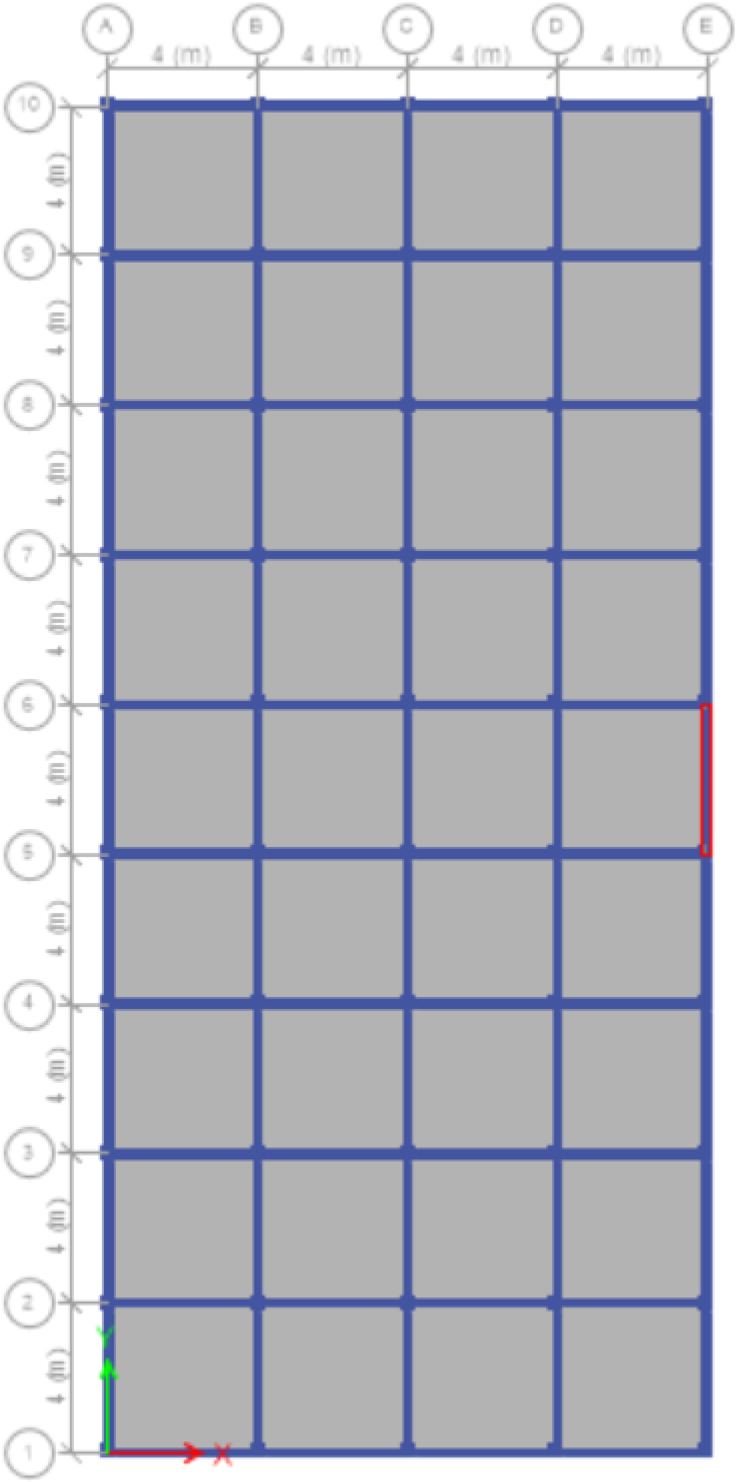

[

: SAP2000 plan view — [M4— 4×9 bays, Lx = 16 m, Ly = 36 m]

Figure A.4 – SAP2000 plan view, Model M4.

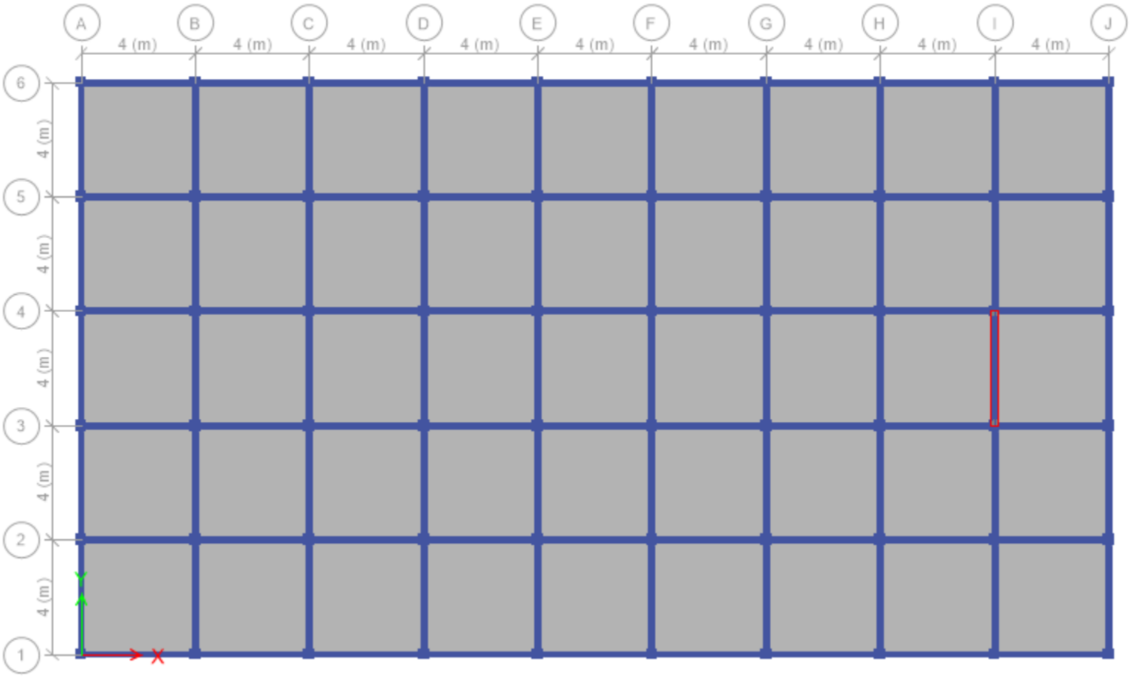

[:

SAP2000 plan view — M5 — 9×5 bays, Lx = 36 m, Ly = 20 m]

Figure A.5 – SAP2000 plan view, Model M5.

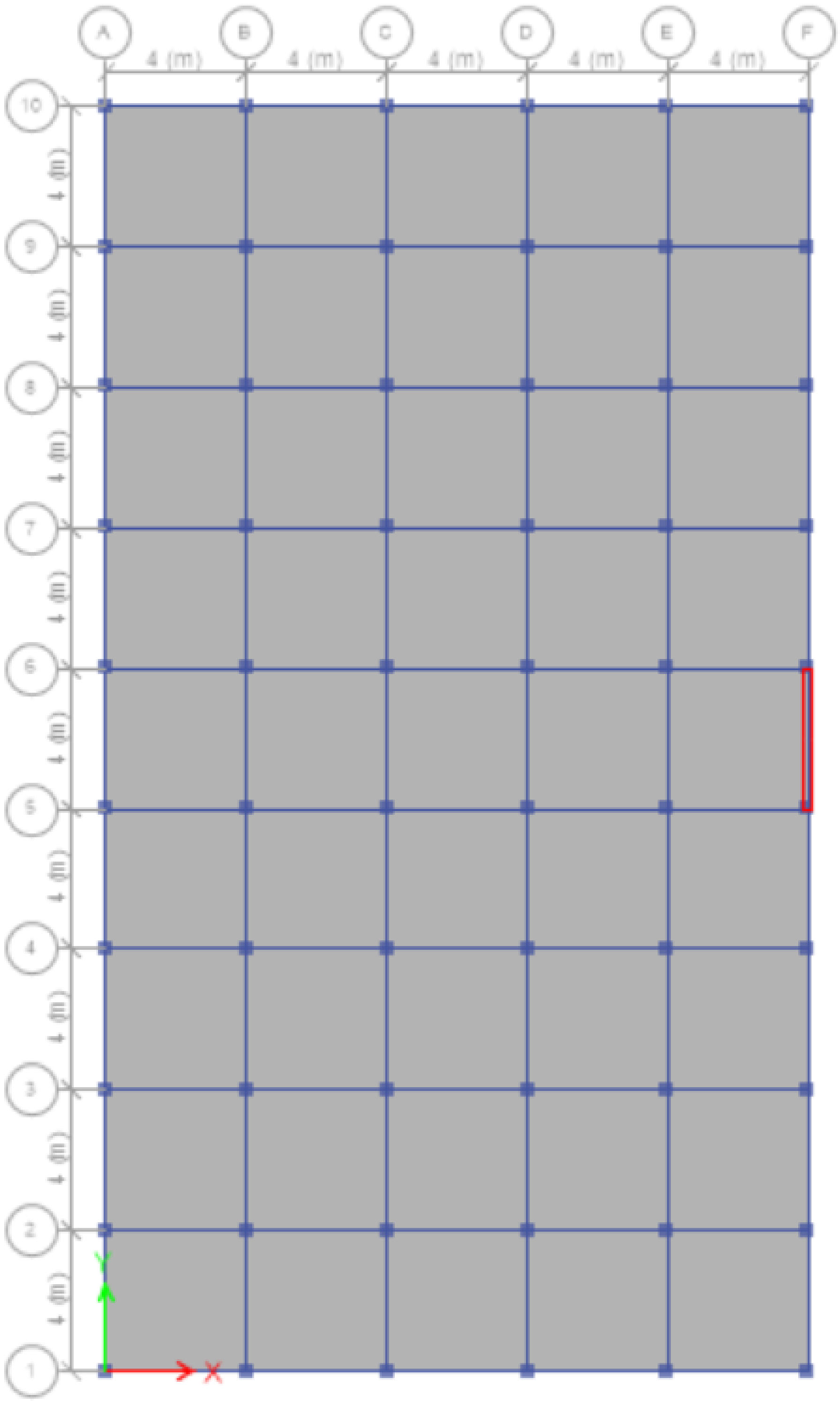

[: SAP2000 plan

[view — M6 — 5×9 bays, Lx = 20 m, Ly = 36 m]

Figure A.6 – SAP2000 plan view, Model M6.

Appendix B – Complete Results

Model	uy,C	uy,F	SAP AF	Orig AF	Orig Err	Mod1 AF	Mod1 Err	Mod1+2 AF	Mod1+2 Err
M1	0.537	0.500	0.931	0.746	24.8%	0.774	20.2%	0.886	5.1%
M2	0.286	0.256	0.895	0.674	32.8%	0.699	28.0%	0.624	43.4%
M3	0.143	0.174	1.217	0.898	35.6%	0.947	28.5%	0.892	36.5%
M4	0.172	0.104	0.605	0.529	14.3%	0.568	6.4%	0.507	19.2%
M5	0.143	0.168	1.175	0.883	33.1%	0.928	26.6%	0.865	35.8%
M6	0.137	0.103	0.752	0.610	23.3%	0.655	14.8%	0.596	26.2%

Table B.1 – Complete displacement and amplification factor results.

Appendix C – Wall Stiffness Derivation

Lateral stiffness of the RCC wall (height H = 4 m, length Lw = 4 m, thickness tw = 0.2 m, E = 30 GPa, G = 12.5 GPa):

$$I = tw \cdot Lw^3/12 = 0.2 \times 4^3/12 = 1.067 \times 10^{-3}\ \mathrm{m}^4$$

$$kf = 3 \times 30{\times}10^6 \times 1.067{\times}10^{-3} / 4^3 = 14.96\ \mathrm{kN/mm}$$

$$Av = 0.833 \times 0.2 \times 4 = 0.667\ \mathrm{m}^2$$

$$ks = 12.5{\times}10^6 \times 0.667 / 4 = 2083\ \mathrm{kN/mm}$$

$$1/kw = 1/14.96 + 1/2083 \quad \Longrightarrow \quad kw \approx 14.85\ \mathrm{kN/mm}$$

The combined stiffness kw for these dimensions is approximately 0.75% less than the flexural-only value kf. The correction is especially crucial for walls with smaller H/Lw ratios (squatter walls), because shear deformation contributes more to the overall displacement.

Appendix D — Nomenclature and List of Symbols

All of the main symbols used in this thesis are defined in the order that they appear in the following list. Symbols that only occur locally inside a single section are specified at the beginning of the text and are not repeated here.

AF — Torsional amplification factor; ratio of the flexible-side y-direction displacement in the C+W system to the y-direction displacement of the C system under the same unit lateral force applied at the centre of mass. AF > 1 indicates that the wall amplifies the flexible-side displacement; AF < 1 indicates that the wall reduces it.

AF_SAP — Numerically computed amplification factor from SAP2000 linear static analysis, defined as AF_SAP = uy,F / uy,C.

AF_Eq4 — Analytically computed amplification factor from Eq. (4) using the specified wall stiffness model and polar stiffness formulation.

bx — Number of bays in the x-direction. The number of column lines in x is bx + 1.

by — Number of bays in the y-direction. The number of column lines in y is by + 1.

C — Reference structural system consisting of n columns arranged on a regular rectangular grid, with no wall.

C+W — Modified structural system obtained from C by adding a single reinforced concrete wall at x = Lx, parallel to the y-direction.

CM — Centre of mass. For a uniform rigid diaphragm, coincides with the geometric centroid of the plan, at coordinates (Lx/2, Ly/2).

CS or CK — Centre of stiffness. For the C system, coincides with the plan centroid. For the C+W system, shifts toward x = Lx by an amount depending on the wall-to-column stiffness ratio.

dx — Bay width in the x-direction, dx = Lx/bx.

dy — Bay width in the y-direction, dy = Ly/by.

E — Elastic modulus of concrete. Taken as E = 30 GPa in all models.

eK — Structural eccentricity; x-direction distance between the centre of mass and the centre of stiffness of the C+W system. Always negative when the wall is at $x = Lx$, indicating that the centre of stiffness is to the right of the centre of mass.

Error — Percentage error in the analytical prediction: Error = $|AF\_SAP - AF\_Eq4| / AF\_SAP \times 100\%$.

Ex,c — x-direction distance from the centroid of the column grid to the rightmost column. For a symmetric grid with bay width dx, $Ex,c = Lx/2$.

Fy — Applied lateral force in the y-direction, taken as a unit force $Fy = 1$ kN in all analyses.

G — Shear modulus of concrete. Taken as $G = E/(2(1+\nu)) \approx 12.5$ GPa for $\nu = 0.2$.

H — Storey height; height of columns and wall. Taken as $H = 4$ m in all models.

I — Second moment of area of the column cross-section about the bending axis. For a square cross-section of side b, $I = b^4/12$.

I_w — Second moment of area of the wall cross-section about the bending axis (parallel to the loading direction y). For a rectangular cross-section of thickness tw and length Lw, $I\_w = tw \cdot Lw^3/12$.

$Icont$ — Continuous approximation of the polar stiffness per unit kc: $Icont = (Lx^2+Ly^2)/12$.

$Idisc$ — Discrete polar stiffness per unit kc: $Idisc = (1/n)\cdot\Sigma_i(xi^2+yi^2)$.

Ipk,C — Polar stiffness of the column system about the centre of stiffness. In the original formula, approximated as $Ipk,C = kc\cdot(Lx^2+Ly^2)/12$. In Modification 2, computed as $Ipk,C = (1/n)\cdot\Sigma_i\, kc\cdot(xi^2+yi^2)$.

Ix — x-direction contribution to the discrete polar stiffness: $Ix = (kc/n)\cdot\Sigma_i\, xi^2$.

Iy — y-direction contribution to the discrete polar stiffness: $Iy = (kc/n)\cdot\Sigma_i\, yi^2$.

kc — Lateral stiffness of a single column in both x and y directions. For a fixed-fixed prismatic column, $kc = 12EI/H^3$.

kf — Flexural stiffness of the wall: $kf = 3EI\_w/H^3$.

ks — Shear stiffness of the wall: $ks = G\cdot Av/H$, where $Av = 0.833\cdot tw\cdot Lw$ is the effective shear area.

k_w — Combined (flexural + shear) wall stiffness: $1/k_w = 1/k_f + 1/k_s$.

$k_{y,c}$ — Total column stiffness in the y-direction: $k_{y,c} = n \cdot k_c$.

$k_{y,w}$ — Wall lateral stiffness in the y-direction; equal to k_f (original formula and reference) or k_w (Modification 1).

$k_{\theta,w}$ — Torsional stiffness contribution of the wall; enters the denominator of the eccentricity term in Eq. (4).

L_w — Length (depth) of the wall cross-section parallel to the y-direction. Taken as $L_w = 4$ m in all models.

L_x — Total plan dimension in the x-direction: $L_x = b_x \cdot d_x$.

L_y — Total plan dimension in the y-direction: $L_y = b_y \cdot d_y$.

M1 to M6 — Labels for the six parametric structural models investigated in this thesis, in order of increasing L_y/L_x from M3 ($L_y/L_x = 0.50$) through M1 ($L_y/L_x = 1.00$) to M4 ($L_y/L_x = 2.25$).

n — Total number of columns: $n = (b_x+1)\cdot(b_y+1)$.

t_w — Thickness of the wall cross-section perpendicular to the y-direction. Taken as $t_w = 0.2$ m in all models.

$u_{y,C}$ — y-direction lateral displacement at the master joint of the reference system C under unit lateral force: $u_{y,C} = F_y/(n \cdot k_c)$ analytically.

$u_{y,F}$ — y-direction lateral displacement at the flexible-side corner joint ($x=0$, $y=0$) of the C+W system under unit lateral force.

x_i — x-coordinate of column i, measured from the centre of stiffness of the column-only system (at $x = L_x/2$). $x_i = -L_x/2 + i \cdot d_x$ for $i = 0, 1, ..., b_x$ (repeated for all b_y+1 rows).

y_i — y-coordinate of column i, measured from the centre of stiffness of the column-only system (at $y = L_y/2$). $y_i = -L_y/2 + j \cdot d_y$ for $j = 0, 1, ..., b_y$ (repeated for all b_x+1 columns).

θ — Rotation of the rigid diaphragm about the vertical axis through the centre of stiffness under the applied lateral force.

ν — Poisson's ratio of concrete. Taken as $\nu = 0.2$ in all models, giving $G = E/2.4 \approx 12.5$ GPa.

Appendix E — Continuous and Discrete Polar Stiffness Evaluation

E.1 Introduction

This appendix derives and compares the continuous and discrete formulations used to evaluate the polar stiffness of the column system. The aim is to isolate the geometric effect of column layout on the analytical equation itself, separately from Chapter 6's assessment of how that geometry ultimately affects the predicted amplification factor.

E.2 Continuous Formulation

The original analytical model evaluates the polar stiffness as

$$\mathrm{Ipk,CS,cont} = \mathrm{Kc,tot} \cdot (\mathrm{Lx}^2 + \mathrm{Ly}^2) / 12$$

where the geometric term is derived from the second moment of area of a uniformly distributed rectangular surface (Section 3.2, Eq. 3.3).

E.3 Discrete Formulation

The proposed formulation evaluates the polar stiffness directly from the coordinates of the individual columns,

$$\mathrm{Ipk,CS,disc} = \Sigma_i\, \mathrm{kc} \cdot (\mathrm{xi}^2 + \mathrm{yi}^2) = \mathrm{Kc,tot} \cdot [(1/n) \cdot \Sigma_i\, (\mathrm{xi}^2 + \mathrm{yi}^2)]$$

showing that only the geometric term differs from the original formulation (Section 3.6, Eq. 3.11).

E.4 Excel Parametric Study

The analytical expressions were implemented in Microsoft Excel for both square and rectangular structural grids at a constant bay spacing of 4 m. The spreadsheet automatically calculates the continuous and discrete polar stiffness values together with the percentage difference between the two formulations for increasing numbers of columns, from n = 9 up to n = 1,000,000. Table E.1 and Table E.2 reproduce a representative subset of the results; the complete dataset (18 square-grid cases and 43 rectangular-grid cases) is given in Appendix F.

Grid	n	Idisc /kc	Icont /kc	Diff. (%)
3×3	9	192	96.0	50.0%
5×5	25	1,600	1,067	33.3%
8×8	64	10,752	8,363	22.2%
11×11	121	38,720	32,267	16.7%
15×15	225	134,400	117,600	12.5%
20×20	400	425,600	385,067	9.5%
100×100	10,000	2.666×10^{8}	2.614×10^{8}	2.0%
1000×1000	10^{6}	2.667×10^{12}	2.661×10^{12}	0.2%

Table E.1 — Square-grid convergence results (representative selection).

Grid (Nx×Ny)	Lx (m)	Ly (m)	n	Idisc /kc	Icont /kc	Diff. (%)
4×2	12	4	8	192	107	44.4%
4×9	12	32	36	4,560	3,504	23.2%
6×5	20	16	30	2,360	1,640	30.5%
10×8	36	28	80	17,280	13,867	19.8%
20×5	76	16	100	56,400	50,267	10.9%
20×10	76	36	200	132,800	117,867	11.2%

Table E.2 — Rectangular-grid convergence results (representative selection).

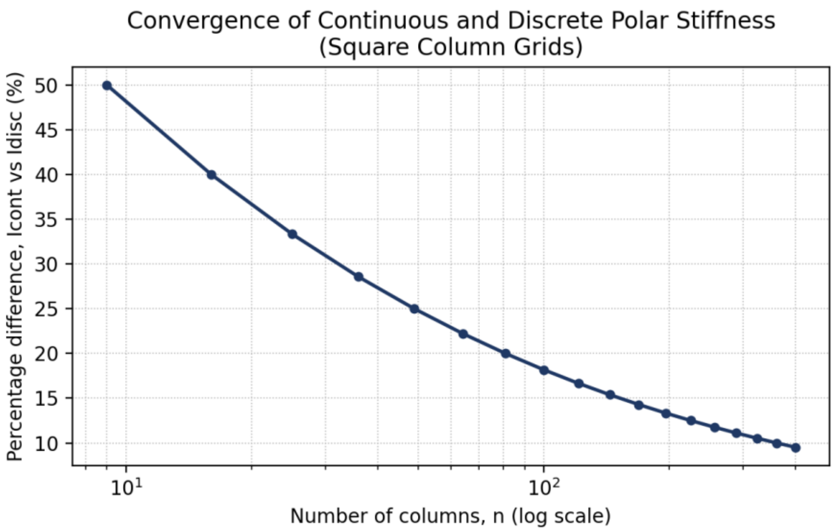

Figure E.1 — Convergence of continuous and discrete polar stiffness, square column grids.

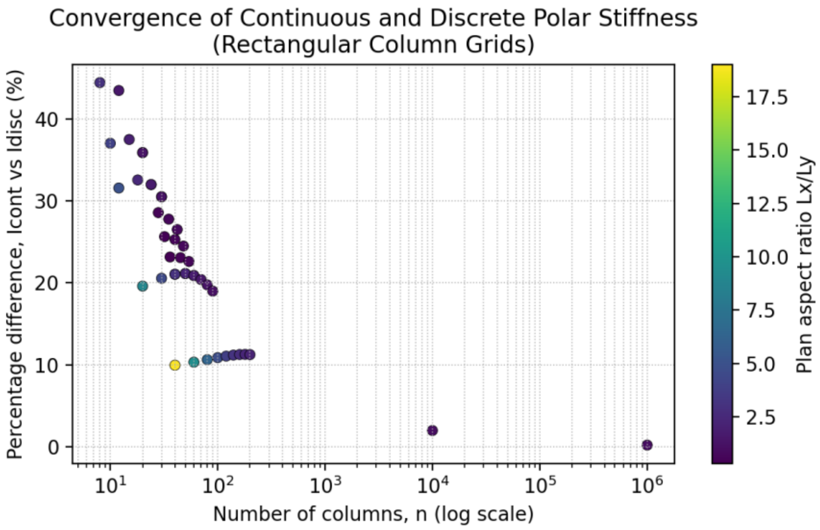

Figure E.2 — Convergence of continuous and discrete polar stiffness, rectangular column grids.

E.5 Discussion

The percentage difference falls off monotonically as column count increases, for both square and rectangular grids. Coarse grids are where the discrete formulation earns its keep, giving a noticeably more accurate picture of the actual column layout; as the grid gets denser, that advantage shrinks, with the discrete values converging on the continuous approximation. This confirms that the continuous formulation is simply the limiting case of the exact discrete solution as column spacing tends to zero relative to the plan dimensions.

This appendix establishes the geometric relationship between the two formulations only. Their different effects on the predicted displacement amplification factor once substituted into Eq. (4) — which is not monotonic in the same way, and depends on the plan aspect ratio rather than on the size of the percentage difference reported here — are examined using the six SAP2000 models in Section 6.4.

Appendix F — Parametric Analysis: Rectangular Structural Plans (Bay spacing s = 4m)

Square plans

Case Label	Columns X (Nx)	Columns Y (Ny)	Bays X	Bays Y	Lx (m)	Ly (m)	Ip,kc_discrete	Ip,kc_continuous	Difference (%)
3x3 Columns	3	3	2	2	8.0	8.0	192.00	96.00	50.00%
4x4 Columns	4	4	3	3	12.0	12.0	640.00	384.00	40.00%
5x5 Columns	5	5	4	4	16.0	16.0	1,600.00	1,066.67	33.33%
6x6 Columns	6	6	5	5	20.0	20.0	3,360.00	2,400.00	28.57%
7x7 Columns	7	7	6	6	24.0	24.0	6,272.00	4,704.00	25.00%
8x8 Columns	8	8	7	7	28.0	28.0	10,752.00	8,362.67	22.22%
9x9 Columns	9	9	8	8	32.0	32.0	17,280.00	13,824.00	20.00%
10x10 Columns	10	10	9	9	36.0	36.0	26,400.00	21,600.00	18.18%
11x11 Columns	11	11	10	10	40.0	40.0	38,720.00	32,266.67	16.67%

12x12 Columns	12	12	11	11	44.0	44.0	54,912.00	46,464.00	15.38%
13x13 Columns	13	13	12	12	48.0	48.0	75,712.00	64,896.00	14.29%
14x14 Columns	14	14	13	13	52.0	52.0	101,920.00	88,330.67	13.33%
15x15 Columns	15	15	14	14	56.0	56.0	134,400.00	117,600.00	12.50%
16x16 Columns	16	16	15	15	60.0	60.0	174,080.00	153,600.00	11.76%
17x17 Columns	17	17	16	16	64.0	64.0	221,952.00	197,290.67	11.11%
18x18 Columns	18	18	17	17	68.0	68.0	279,072.00	249,696.00	10.53%
19x19 Columns	19	19	18	18	72.0	72.0	346,560.00	311,904.00	10.00%
20x20 Columns	20	20	19	19	76.0	76.0	425,600.00	385,066.67	9.52%

Rectangular plans

Case Label	Columns X (Nx)	Columns Y (Ny)	Bays X	Bays Y	Lx (m)	Ly (m)	Ip,kc_discrete	Ip,kc_continuous	Difference (%)
4x2 Columns	4	2	3	1	12.0	4.0	192.00	106.67	44.44%

4x3 Columns	4	3	3	2	12.0	8.0	368.00	208.00	43.48%
4x5 Columns	4	5	3	4	12.0	16.0	1,040.00	666.67	35.90%
4x6 Columns	4	6	3	5	12.0	20.0	1,600.00	1,088.00	32.00%
4x7 Columns	4	7	3	6	12.0	24.0	2,352.00	1,680.00	28.57%
4x8 Columns	4	8	3	7	12.0	28.0	3,328.00	2,474.67	25.64%
4x9 Columns	4	9	3	8	12.0	32.0	4,560.00	3,504.00	23.16%
4x10 Columns	4	10	3	9	12.0	36.0	6,080.00	4,800.00	21.05%
5x2 Columns	5	2	4	1	16.0	4.0	360.00	226.67	37.04%
5x3 Columns	5	3	4	2	16.0	8.0	640.00	400.00	37.50%
5x4 Columns	5	4	4	3	16.0	12.0	1,040.00	666.67	35.90%
5x6 Columns	5	6	4	5	16.0	20.0	2,360.00	1,640.00	30.51%
5x7 Columns	5	7	4	6	16.0	24.0	3,360.00	2,426.67	27.78%
5x8 Columns	5	8	4	7	16.0	28.0	4,640.00	3,466.67	25.29%
5x9 Columns	5	9	4	8	16.0	32.0	6,240.00	4,800.00	23.08%
5x10 Columns	5	10	4	9	16.0	36.0	8,200.00	6,466.67	21.14%
6x2 Columns	6	2	5	1	20.0	4.0	608.00	416.00	31.58%
6x3 Columns	6	3	5	2	20.0	8.0	1,032.00	696.00	32.56%
6x4 Columns	6	4	5	3	20.0	12.0	1,600.00	1,088.00	32.00%

6x5 Columns	6	5	5	4	20.0	16.0	2,360.00	1,640.00	30.51%
6x7 Columns	6	7	5	6	20.0	24.0	4,648.00	3,416.00	26.51%
6x8 Columns	6	8	5	7	20.0	28.0	6,272.00	4,736.00	24.49%
6x9 Columns	6	9	5	8	20.0	32.0	8,280.00	6,408.00	22.61%
6x10 Columns	6	10	5	9	20.0	36.0	10,720.00	8,480.00	20.90%
10x2 Columns	10	2	9	1	36.0	4.0	2,720.00	2,186.67	19.61%
10x3 Columns	10	3	9	2	36.0	8.0	4,280.00	3,400.00	20.56%
10x4 Columns	10	4	9	3	36.0	12.0	6,080.00	4,800.00	21.05%
10x5 Columns	10	5	9	4	36.0	16.0	8,200.00	6,466.67	21.14%
10x6 Columns	10	6	9	5	36.0	20.0	10,720.00	8,480.00	20.90%
10x7 Columns	10	7	9	6	36.0	24.0	13,720.00	10,920.00	20.41%
10x8 Columns	10	8	9	7	36.0	28.0	17,280.00	13,866.67	19.75%
10x9 Columns	10	9	9	8	36.0	32.0	21,480.00	17,400.00	18.99%
20x2 Columns	20	2	19	1	76.0	4.0	21,440.00	19,306.67	9.95%
20x3 Columns	20	3	19	2	76.0	8.0	32,560.00	29,200.00	10.32%
20x4 Columns	20	4	19	3	76.0	12.0	44,160.00	39,466.67	10.63%
20x5 Columns	20	5	19	4	76.0	16.0	56,400.00	50,266.67	10.87%
20x6 Columns	20	6	19	5	76.0	20.0	69,440.00	61,760.00	11.06%

20x7 Columns	20	7	19	6	76.0	24.0	83,440.00	74,106.67	11.19%
20x8 Columns	20	8	19	7	76.0	28.0	98,560.00	87,466.67	11.26%
20x9 Columns	20	9	19	8	76.0	32.0	114,960.00	102,000.00	11.27%
20x10 Columns	20	10	19	9	76.0	36.0	132,800.00	117,866.67	11.24%